applied sciences

MDPI

Review

Hollow-Core Optical Fibers for Telecommunications and Data Transmission

Krzysztof Borzycki [1,*] and Tomasz Osuch [1,2]

[1] National Institute of Telecommunications, 04-894 Warsaw, Poland; tomasz.osuch@pw.edu.pl
[2] Faculty of Electronics and Information Technology, Institute of Electronic Systems, Warsaw University of Technology, 00-665 Warsaw, Poland
* Correspondence: k.borzycki@il-pib.pl; Tel.: +48-22-5128-124

Abstract: Hollow-core optical fibers (HCFs) have unique properties like low latency, negligible optical nonlinearity, wide low-loss spectrum, up to 2100 nm, the ability to carry high power, and potentially lower loss then solid-core single-mode fibers (SMFs). These features make them very promising for communication networks and similar applications. However, this class of fibers is still in development. Current applications are almost exclusively limited to low-latency data links for High-Speed Trading (HST); other uses are in the trial stage now. In this paper, we comprehensively review the progress in the development of HCFs including fiber design, fabrication and parameters (with comparisons to conventional single-mode fibers) and support technologies like splicing and testing. A variety of HCF applications in future telecom networks and systems is analyzed, pointing out their strengths and limitations. Additionally, we review the influence of filler gas and entry of contaminants on HCF attenuation, and propose a new fusion splicing technique, avoiding the destruction of the fiber's photonic cladding at high temperature.

Keywords: hollow-core fiber; photonic bandgap fiber; anti-resonant fiber; nested anti-resonant nodeless fiber; latency; telecommunications; data transmission; DWDM; optical fiber splicing

check for updates

Citation: Borzycki, K.; Osuch, T. Hollow-Core Optical Fibers for Telecommunications and Data Transmission. *Appl. Sci.* **2023**, *13*, 10699. https://doi.org/10.3390/app131910699

Academic Editors: John Xiupu Zhang and Chi-Wai Chow

Received: 12 July 2023
Revised: 18 September 2023
Accepted: 22 September 2023
Published: 26 September 2023

Copyright: © 2023 by the authors. Licensee MDPI, Basel, Switzerland. This article is an open access article distributed under the terms and conditions of the Creative Commons Attribution (CC BY) license (https://creativecommons.org/licenses/by/4.0/).

1. Introduction

Despite the impressive development of conventional optical fibers with a solid core and cladding since the publication of Kao and Hockham's paper in 1966 [1], and the emergence of fibers such as the dominant wired transmission medium, with approx. 550 million km installed in 2022, new fibers for communication networks are being developed, in particular multi-core fibers (MCFs) with high core density [2,3], and hollow-core fibers.

The main driver of HCF development is bypassing limitations imposed by the properties of fused silica (SiO_2). Affected parameters include, in particular, the following:

- Minimum attenuation: 0.14–0.16 dB/km @ 1550 nm;
- Low-loss bandwidth: ≈1250–1750 nm, or ≈68 THz @ ≤ 0.40 dB/km;
- Latency and effective refractive index: n_{eff} = 1.45–1.47;
- Optical nonlinearities, in particular Kerr, Raman and Brillouin effects;
- Maximum optical power carried by fiber without damage.

These limitations do not exist in hollow-core fibers, where the bulk of guided radiation propagates in gas and the interaction of this radiation with glass is limited by a factor of 100–100,000 in comparison to that of solid-core fibers, depending on the particular HCF [4,5].

We review unique advantages brought on by the use of HCFs in communication networks, data transmission, data centers, radio facilities, etc. HCFs, like most novelties, will initially be expensive but are adopted when one or both of the following conditions are met:

- The length and cost of fiber needed is low in comparison to the economic or other benefits obtained (acceptable cost/benefit ratio);
- Technical requirements cannot be met using traditional fibers. Examples include mid-infrared transmission ($\lambda \geq 1.75$ μm), phase-sensitive systems operating in variable temperatures, high-power applications, and systems affected by backscattering.

Issues currently preventing wide adoption of HCFs in telecom networks are also reviewed, with possible solutions.

Prospective applications of hollow-core fibers, apart from HST, include the linking of antennae at microwave radio sites, high-capacity DWDM networks, radiation-resistant data links, supercomputers, radars with phased antenna arrays and short synchronization links. Adoption in more cost-sensitive facilities like data centers, LANs, or 5G networks will likely wait for large-scale manufacturing and lower cost of fibers.

This review is mostly limited to dielectric HCFs made of fused silica, as fibers made of other materials lack an adequate optical and mechanical performance, in particular, attenuation low enough for transmission over kilometer distances. Applications other than transmission in telecom and data systems, like sensors and power delivery, are not covered.

The rest of this paper is arranged as follows. The main types of hollow-core fibers are introduced in Section 2, and reviewed in more detail later: Bragg fibers in Section 3, photonic bandgap fibers in Section 4, and anti-resonant fibers in Section 5. In Section 6, the consequences of changing the optical transmission medium from glass or polymer to gas are briefly presented, including issues like gas impurities and water penetration into HCF.

Selected properties and parameters of HCFs important for communication networks are reviewed in Section 7, with comparison to solid-core single-mode fibers. The most important models of the guiding mechanism in HCFs and simulation tools are presented in Section 8, while manufacturing is shortly looked at in Section 9. The splicing and termination of HCFs are described in Section 10. Transmission properties of HC-PBGF and NANF fibers are evaluated in Section 11. Possible applications of HCFs are reviewed in Section 12, and some technologies required for deployment of HCFs in networks in Section 13. The conclusions are presented in Section 14.

2. Main Types of Hollow-Core Fibers

2.1. Basic Designs

Dielectric hollow-core fibers include central round, gas-filled cavity (core) surrounded by a photonic barrier (cladding), preventing the escape of radiation. HCFs were first proposed in 1976 (Bragg slab waveguides) [6], 1978 (Bragg fibers) [7] and 1995 (Photonic Bandgap Fiber-PBGF) [8]. Fibers developed so far can be split into three groups depending on the light confinement mechanism employed:

(a) Bragg Fibers, where the core is enclosed with multiple alternating layers of transparent materials with high and low refractive index constituting a Bragg mirror (Figure 1a);
(b) Hollow-core Photonic Bandgap Fibers (HC-PBGFs), where multiple layers of periodic glass/air structure around the core block the radial propagation of light (Figure 1b). PBGFs with solid core are not covered here;
(c) Anti-Resonant Fibers (ARFs), where the optical anti-resonance in multiple flat membranes or walls of tubes blocks the radial propagation of light. (Figure 1c).

In fibers (b) and (c), the structure blocking escape of light (cladding) is normally made of gas and pure fused silica; other glasses and polymers are less useful, primarily due to low mechanical strength and gas permeability.

The first anti-resonant fibers were Kagome fibers, where the cladding is a lattice of hexagonal and triangular cells (Figure 2a). This fiber was modified by changing the surfaces around fiber's core from flat to curved ones, resulting in "negative curvature" fiber (Figure 2b), reduced overlap of guided light with glass, and lower loss [9,10]. Further development led to the replacement of Kagome cladding with a single layer of thin-walled, single or nested glass tubes, resulting in NANF fibers (Figure 1c). [11].

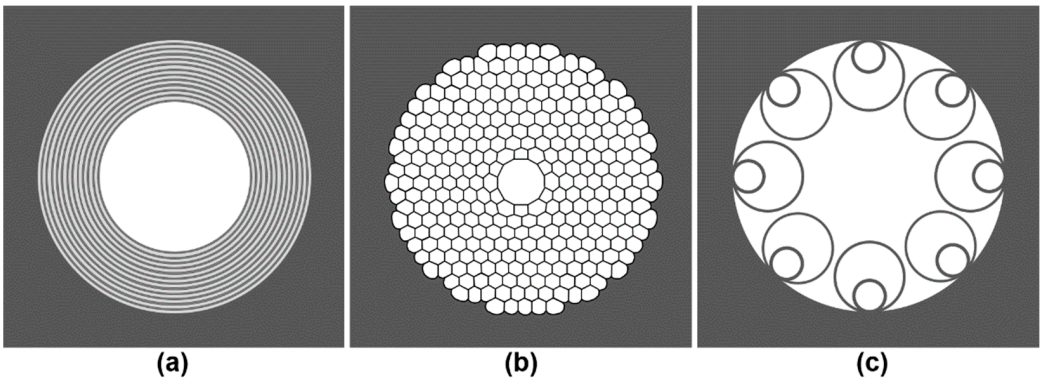


Figure 1. Structures of HCFs: (**a**) Bragg Fiber; (**b**) Photonic Bandgap Fiber (Blaze Photonics HC-1550-02); (**c**) Anti-Resonant fiber of NANF type. Filling gas is shown as white, fused silica as dark grey. In the left drawing, lighter and darker shades of grey indicate low-index and high-index materials of the Bragg reflector. Outer part of cladding and protective coating not shown.

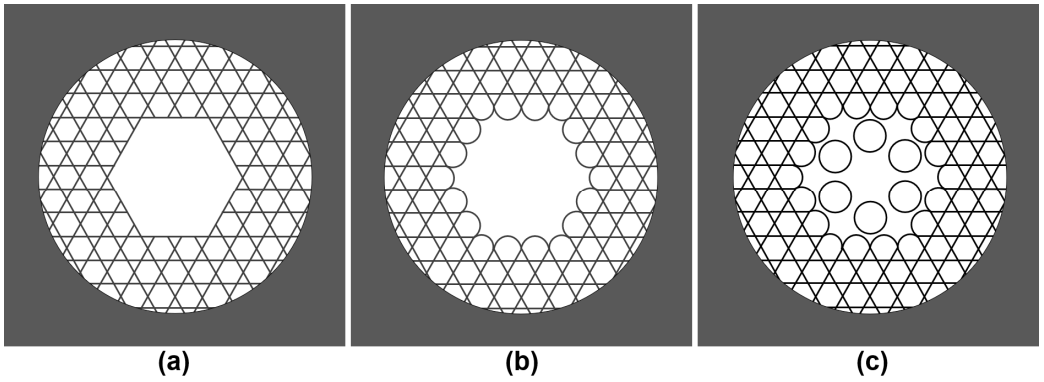


Figure 2. HCFs with Kagome lattice: (**a**) "pure" Kagome; (**b**) with "negative curvature" surfaces towards core; (**c**) with hybrid lattice including "levitating" anti-resonant capillaries (right). Drawings show ideal structures without distortions introduced during consolidation of preform and drawing of fiber.

2.2. Main Differences

All hollow-core fibers, except for capillary fibers with metallic mirror, not discussed here, exhibit low-loss guidance of radiation in specific bands of wavelengths only, depending on the refractive index of materials used and the geometry of the light-guiding structure. Fibers of type (c) with nested capillaries (Nested Anti-resonant Nodeless Fiber-NANF) can have low-loss bandwidth of several hundred nanometers [12].

HC-PBGF fibers (Figure 1b) have a photonic barrier exhibiting periodic variation in the refractive index, made of multiple concentric layers of identical, usually hexagonal, gas-filled cells, sometimes called a "photonic crystal", because of regularly repeating units and their directional arrangement. The typical number of layers is 6–9. All solid parts of this fiber are made of the same material.

The first HC-PBGF was reported in 1999 [11]. The fabrication of such a fiber using the "stack-and-draw" method is difficult (Section 9), mostly due to the following factors:

- Assembling large number of tubes (263 for fiber in Figure 1b) is labor-intensive and requires clean room;
- The dimensions of parts change during the consolidation of preform and the drawing of fiber due to the surface tension of softened glass and variations in the gas pressure in tubes.

Low-loss bandwidth of HC-PBGF can be considerably reduced via interference from lossy surface modes localized at the core–cladding interface; these modes can anti-cross

with air-guided modes, giving rise to narrow spectral regions of high loss [11]. Examples of loss spectra are shown in Section 4.1.

Kagome fibers have a very characteristic photonic structure, including a combination of hexagonal and triangular cells, with two triangular cells adjacent to each larger hexagonal one (Figure 2). Kagome is a name used in Japan for a hexagonal weaving pattern. Despite the superficial similarity to HC-PBGF, the escape of light from the core is blocked by anti-resonance (Section 5.1), not a photonic bandgap. Kagome fibers have wider bandwidth than HC-PBGFs, but the blocking of light escape is usually less effective and fiber attenuation higher. Number of preform parts is comparable.

Loss can be reduced in hybrid Kagome designs (Figure 2b,c) via the addition of "negative curvature" parts (bulges) and/or single or nested tubes constituting additional, nodeless structures around the cavity, at the expense of more complex manufacturing [11]. Thin supports for "levitating" tubes (Figure 2c), not shown due to fine dimensions, reduce undesirable light scattering, but can break when the fiber is sharply bent or twisted.

The lowest attenuation was achieved in NANFs: similar to, at 1550–1600 nm, and lower, at $\leq$1350 nm, than in the best solid-core fibers [12,13].

Specific types of HCFs are presented in Sections 3–5, with a focus on properties important for communication networks and data transmission, in particular improvements over conventional (solid) fused silica fibers.

3. Bragg Fibers

An optical hollow slab waveguide lined with a Bragg reflector was proposed in 1976 by Yeh and Yariv [6]. In 1978, Yeh, Yariv, and Marom analyzed how to design a cylindrical optical fiber with a Bragg reflector around a central cavity [7], finding that "*it is possible, in principle, to fabricate optical fibers with a multiannulus cladding whose indices may be higher than that of a core. Such fibers are strongly mode selective and can operate single mode even with large core diameter.*"

The next step was made at MIT, where Joel Fink et al. made and tested a Bragg fiber [14], utilizing experience gained during earlier work for the U.S. Air Force on dielectric "perfect mirror" coatings, making aircraft stealthy at infrared wavelengths.

As shown in Figure 1 (left), the fiber's central cavity (core) is surrounded by cladding made of alternating layers of transparent, dielectric materials with very different refractive indices, ($n_1 > n_2$) constituting a Bragg reflector, which prevents the escape of radiation propagating in this cavity. High index layers are thinner, roughly in proportion to the ratio of indices. Each pair of layers has a combined thickness of half a wavelength:

$$d_1 n_1 + d_2 n_2 = N\lambda/2, \quad (1)$$

where d_1 and d_2 are the thicknesses of each layer, n_1 and n_2 denote their refractive indices, λ is the operating wavelength in a vacuum, and N is an integer number (1, 2, 3, ...). The higher the n_1/n_2 ratio, the smaller is the number of layer pairs for a given reflectivity.

The design of a Bragg reflector for optical fiber is complicated by the requirement that reflection must be ensured for the full range of the fiber's operating wavelengths [7,14] by varying thickness and reflection wavelength for different pairs of layers. The reflector may be a set of concentric cylinders made of fused silica and separated by air gaps. However, to keep the cylinders in place with sub-μm tolerances, each layer of air must be subdivided into narrow cells by struts providing support—in this way, we obtain a hollow-core photonic bandgap fiber, presented in Section 4.

In theory, a hollow-core Bragg fiber (solid-core Bragg fibers also exist) has unique advantages:

(a) The material of the fiber's outer tube (jacket) does not interact with guided radiation; it must only provide mechanical strength and hermeticity,
(b) Bandwidth and attenuation depend solely on the design of the Bragg reflector and the properties of the materials used: refractive index, absorbance, and scattering.

The fiber's bandwidth is adjusted by changing the thickness and number of layers of the Bragg reflector structure, while the absorbance of the materials used can be fairly high due to the limited penetration of guided radiation into them [15].

However, there are severe difficulties in the design and manufacture of Bragg fibers:

- For almost 100% reflection with a low number of layers, usually 8–20 (Figure 3), the difference ("contrast") of the refractive indices must be high, and materials of very different chemical compositions are required. Examples include poly(etherimide) (PEI) or poly(ether sulfone) (PES) as low index materials and arsenic triselenide (As_2Se_3) as a high index material, with n = 1.62 (PEI) and n = 2.73 (As_2Se_3) at 2000 nm, respectively [15,16]. The latter material is also poisonous.
- The materials of the Bragg reflector and cladding (jacket) shall have similar melting temperatures and melt viscosities to allow fiber drawing.

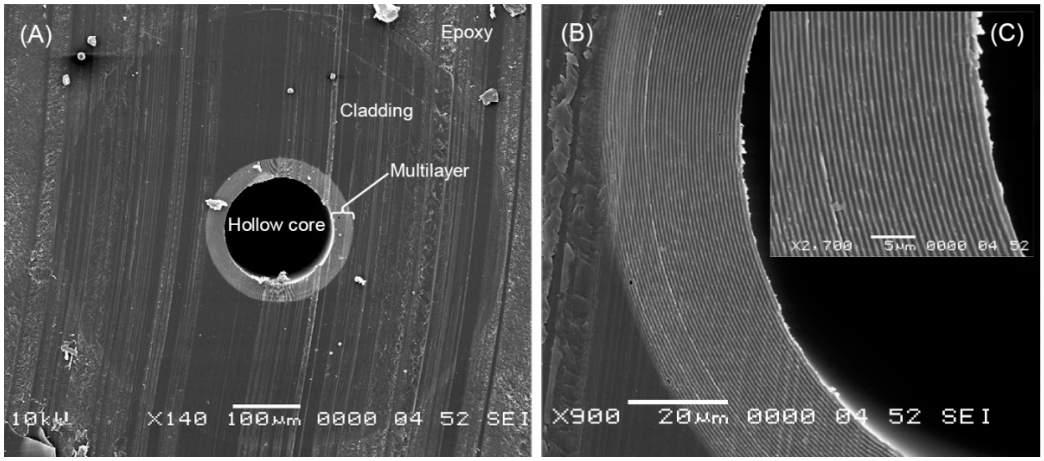


Figure 3. HCF with a Bragg reflector made of 74 alternating layers of PEI polymer, seen as grey (each 0.47 µm thick), and arsenic triselenide, seen as white (each 0.27 µm thick). The cladding had a 684 µm outer diameter and was made of PES polymer. (**A**) complete fiber, (**B**) Bragg reflector, (**C**) layers of Bragg reflector. This fiber had a fundamental photonic bandgap at 2.28 µm. Reproduced from [15].

The thickness of each reflector layer must be precisely controlled, but the preform must include no small voids prone to shrinking and collapsing due to surface tension.

The tedious deposition of numerous layers from solution or vapor phase in a tube can be avoided by making a sheet of dual- or triple-layer foil of the materials required, and winding it the required number of times around a smooth central rod [15]. The rod is later removed, and the jacketing tube applied. Individual layers of foil are consolidated when the preform is heated enough for melting or softening of one or both materials.

The researchers at OmniGuide Communications Inc. published, in 2002, a paper [17] in which they stated that confinement loss can be as low as 0.003 dB/km at 1650 nm for a 17 layer Bragg reflector made of materials with refractive indices of n = 1.6 and n = 4.6. This study, unfortunately, omitted absorption and scattering resulting from contamination, irregularities, and inclusions in the reflector materials. The lowest loss measured in a hollow-core Bragg fiber at a typical telecom wavelength (1570 nm) was ≈5500 dB/km [15], and the interest of most researchers shifted to HC-PBGF and ARF fibers.

4. Photonic Bandgap (Photonic Crystal) Fibers

The theory of light guidance in HC-PBGF and ARF fibers can be found in [18,19]. The key loss mechanisms in HC-PBGFs are presented in [11]. The history of HCF development until 2020, with a focus primarily on loss reduction, and compact descriptions of each guidance mechanism can be found in paper [10].

Technical data, fiber photos, and results of measurements included in Sections 3–5 are collected from the referenced literature, product data sheets, and patent descriptions.

Graphs were drawn by the authors from data in the indicated references to ensure uniform appearance and/or present different fibers or parameters together. In a few cases, data are estimated in the absence of published information and indicated as such.

4.1. Fibers with Regular Photonic Structure

Photonic bandgap fiber was invented by P.J. Russell at the University of Bath in 1991 [12], with a paper about it published in 1995 [8]. The basic idea—surrounding a central part reserved for light propagation (hollow or otherwise) with a periodic photonic structure composed of alternating low- and high-refractive-index materials, blocking the leakage or entry of light due to anti-resonance in periodic nodes (hollow channels)—proved versatile and became the basis for extensive research. HC-PBGF cladding is a periodic, multi-layered structure composed of glass and gas and known as two-dimensional photonic crystal, in the center of which a defect (core) is included. The core is usually made by removing 7, 19, or 37 adjacent cells of this structure—in fact, just the walls between them—forming a circle [10]. Radiation at frequencies within the bandgap cannot pass this cladding (in the radial direction—the bandgap effect is, in general, direction- and polarization-dependent) and is confined to the core and the nearest layers of cladding. The effectiveness of such guidance is limited, and a reduction in leakage loss to less than 1 dB/km usually requires 4–8 layers of cladding.

Unlike conventional solid fibers with high index cores and low index cladding, light guidance in HC-PBGF is narrowband. In practice, the bandgap of a nominally uniform cladding often varies from one layer to another due to the distortion of the fiber structure during the consolidation of the preform. This can be beneficial: multiple layers of cladding with stepped bandgaps extend the low-loss bandwidth of the fiber, although a higher attenuation must be accepted or the number of layers increased.

HC-PBGFs have either a single low-loss band, which can be more than 100 nm wide, or several narrow bands (Figure 4). Multiple narrow bands can be related to the presence of additional large holes in the cladding (Figure 5), introduced to capture and leak away light from higher-order modes.

One direction of HCF development, from early HC-PBGFs to current NANFs, is decreasing the air filling fraction of the cladding from ≈90% to 5–10% in order to reduce overlap between optical power and glass, fiber loss, and nonlinearity—see Sections 6.1 and 6.2.

Attenuation was considerably lower than in Bragg fibers. The loss of early HC-PBGFs, in excess of 1000 dB/km, was reduced to 1.7 dB/km at 1560 nm in 2004 [20] and 1.2 dB/km in 2005 [18] by researchers from the University of Bath, but no further loss reduction in this class of fibers was achieved. Such fibers are suitable for data links in LANs, data centers, or radio sites, but not metro and long-distance networks.

Overall, HC-PBGFs have four serious disadvantages when applications in data transmission and telecom networks are considered:

(a) Propagation of higher-order modes in the photonic cladding, and modal dispersion, even when the core diameter is typical for single-mode fibers (10–20 μm) [21];
(b) High polarization mode dispersion (PMD), frequently in the order of 100 $\sqrt{}$ps/km, resulting from the non-circularity of the core and distortions during consolidation and drawing. A PMD over 55 ps/$\sqrt{}$km was reported for a fiber placed in a loose-tube cable [22–25];
(c) High surface scattering loss (SSL) [26]—see Section 6.2;
(d) Many HC-PBGFs have low loss only in a few narrow (10–30 nm) sections of the spectrum (Figure 4) [20,27,28] because of interference between the lossy surface modes and the fundamental mode [11]. However, fibers of this type with a broad (≈150 nm) transmission bandwidth centered around 1550 nm have been developed.

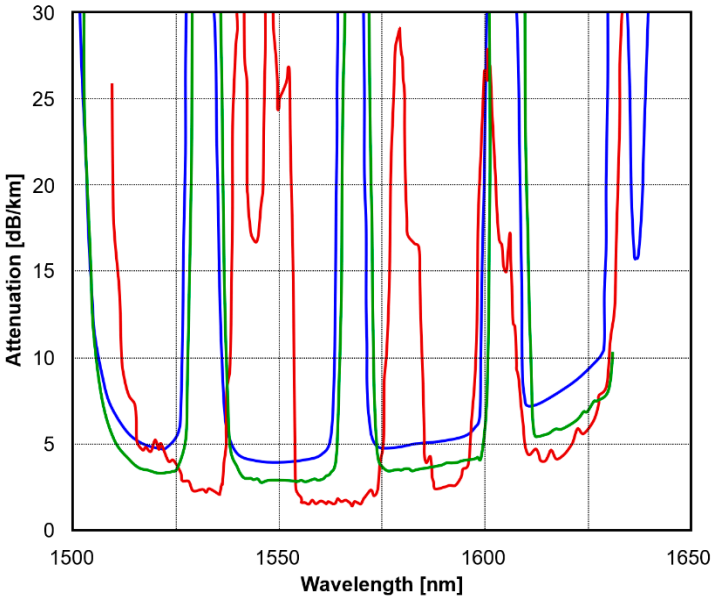


Figure 4. Loss spectra of HC-PBGFs: low-loss experimental fiber (red) [20], and OFS AccuCore fibers with six shunts: typical production fiber (blue) [28], and experimental fiber (green) [22].

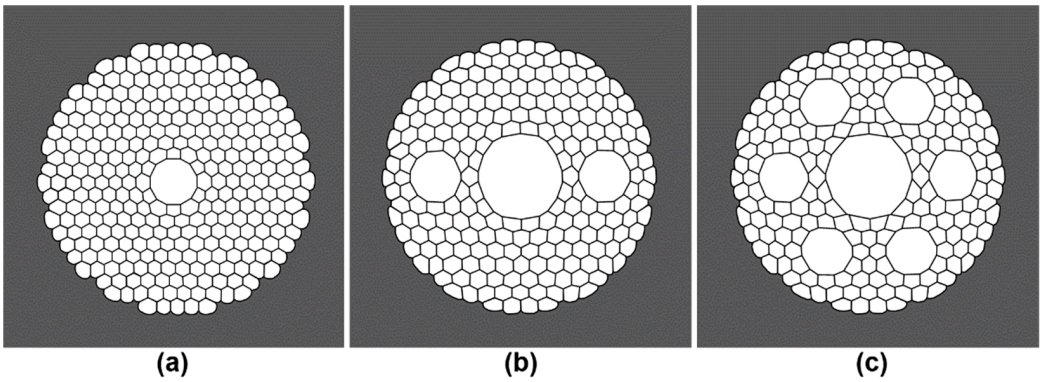


Figure 5. Evolution of HC-PBGF to ensure single-mode operation: (**a**) early design without shunts (Blaze Photonics HC-1550-02); (**b**) OFS single-mode fiber with two shunts [20]; (**c**) OFS AccuCore improved single-mode fiber with six shunts [21,28].

An example of a "wideband" HC-PBGF fiber is NKT Photonics HC-1550, whose data are presented in Table 1. Figures 5a and 6 show gradually variable sizes of holes.

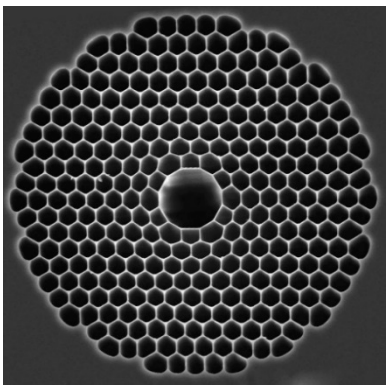


Figure 6. SEM image of NKT Photonics (formerly Blaze Photonics) HC-1550 fiber. Despite overall good control of fiber dimensions during manufacturing, cells in inner layers are noticeably smaller than in outer ones. Image courtesy of NKT Photonics.

Problem (a) was solved with the introduction of shunts in the cladding (see Section 4.2), and problem (b) with the spinning of the fiber during drawing [21,22]. Problems (c) and (d) were eliminated in a new class of HCFs—the anti-resonant fibers (ARFs)—discussed in Section 5.

A fragmented transmission spectrum does not affect transmission at one or few wavelengths, including low-capacity DWDM links [22], but spectrally incompatible fibers cannot be spliced into a joint optical path, e.g., during the expansion of an existing network. Large-core HC-PBGF fibers are not suitable for high capacity DWDM networks, where a low loss at least in a full C-band (≈1528–1565 nm) is required.

To minimize light scattering via surface capillary waves on surfaces around the core, and the resulting component of fiber attenuation (SSL, see Section 6.2) [26], the core diameter of a typical HC-PBGF intended for data transmission is considerably larger than in solid single-mode fibers. For example, the OFS AccuCore fiber [22,27] has core diameter of 25 μm, and an effective cross-section A_{eff} = 200 μm^2, while the widely used single-mode fibers conforming to the ITU-T G.652 standard [29], such as the Corning SMF-28e+ [30] and SMF-28 Ultra [31], have an 8.2 μm core diameter and A_{eff} = 82 μm^2. A large mismatch between the mode field diameters (MFD) of these fibers requires special arrangements during their splicing [27]. Commercial HC-PBGFs are primarily offered as lengths of cable terminated in the factory with pigtails including standard single-mode fibers [28], as described in Section 10.1.

4.2. Single-Mode PBGFs with Shunts

Photonic bandgap fibers with regular photonic cladding support the propagation of higher-order modes, while telecom networks require single-mode fibers. Single-mode propagation can be ensured with "shunts"—hollow cavities larger than normal cells of the photonic structure, but smaller than the core (Figure 5). In the OFS fibers shown in Figure 5b,c [21], the core and shunt have cross-sections equal to 19 cells and 7 cells, respectively.

Shunts are traps for higher-order modes: radiation is accepted by the shunt, but leaks from it through the cladding, escaping the fiber. Shunts are designed such that higher-order modes in the core are phase matched to the fundamental mode in them. The loss experienced by the fundamental mode guided in the core is not significantly affected. After a certain length, e.g., 0.5 m [32], only the fundamental mode effectively propagates, despite the large diameter of core (25 μm in Figure 5b,c). Single-modedness in a six-shunt HC-PBGF can be better than in an SMF, where the cutoff wavelength is tested on longer samples: 2 m (fiber in primary coating) or 22 m (fiber in the cable) [33].

Figure 6 shows the deformation of the photonic structure during fiber manufacturing, in particular at the borders with the core and jacketing tube. Each small cell was originally a round glass tube. One undesirable effect is the lack of radial symmetry, causing PMD.

HCFs and solid-core single-mode fibers exhibit opposite relationship between diameter and the area of the fiber's core and the fundamental mode propagating in it:

- In solid-core fibers, mode field diameter and effective area are larger than the dimensions of the core, as diffraction causes light to "spill" into the cladding;
- In hollow-core fibers, the mode field is "pushed" towards the center of the core, away from the photonic cladding, and MFD is smaller than the core diameter (Table 2);
- The mode field diameter of HC-PBGFs decreases with the wavelength, while that of solid-core fibers increases with the wavelength at similar rate (Figure 7).

Another special property of HC-PBGFs is the characteristic of chromatic dispersion (CD), shown in Figure 8 for OFS AccuCore fiber [22]. Both the CD and CD slopes rapidly increase close to the edges of the transmission band, and the sign of CD is reversed in the middle. As a result, high bit rate transmissions in a part of the low-loss band may require dispersion compensation, which adds undesirable latency.

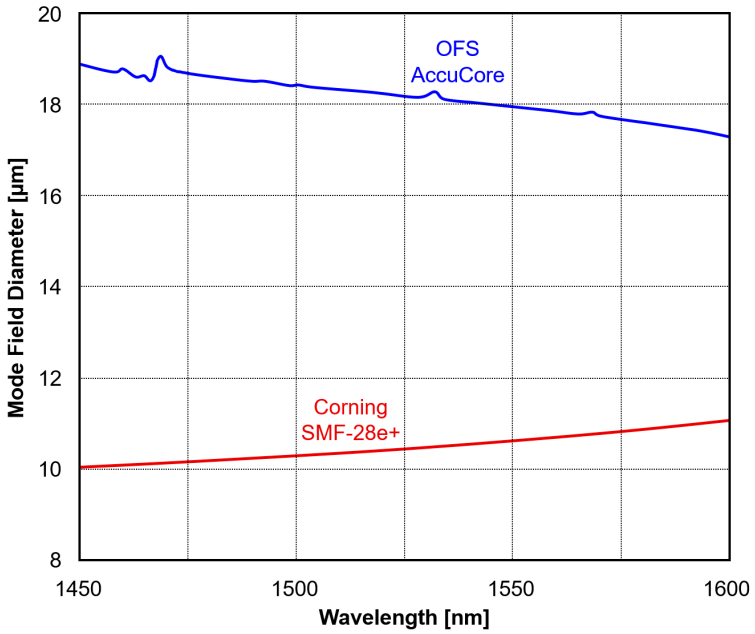


Figure 7. MFD vs. wavelength: OFS AccuCore with six shunts [34] and Corning SMF-28+ [30].

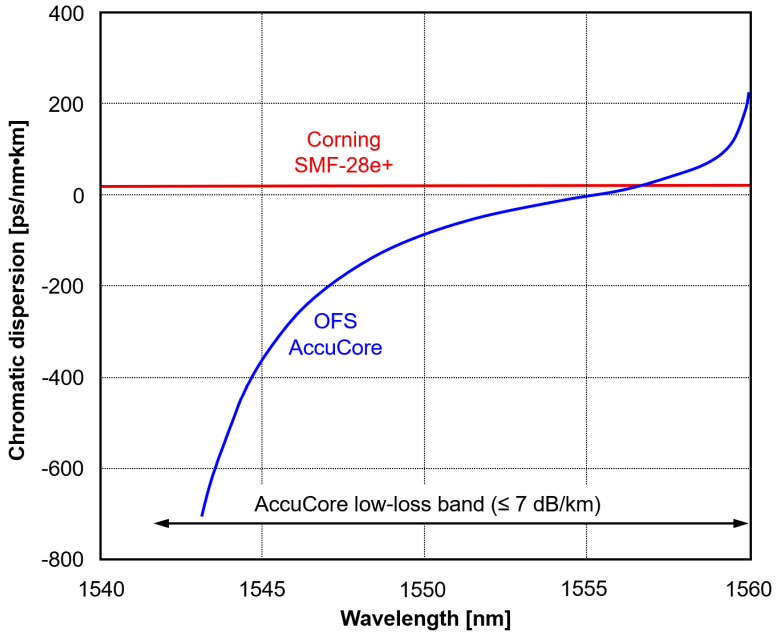


Figure 8. Chromatic dispersion of OFS AccuCore with six shunts—four lengths concatenated [22], and Corning SMF-28e+ [30]. The dispersion of individual lengths of AccuCore differed substantially.

4.3. Commercial Fibers and Their Parameters

The main suppliers of commercial HC-PBGFs are OFS Fitel (a Furukawa group company) in the U.S. and NKT Photonics (a subsidiary of Hamamatsu Photonics K.K.) in Denmark.

Fibers from NKT Photonics share a common design (Figures 5a and 6), tailored for wavelengths between 800 nm and 1550 nm by sizing of core and photonic cladding. HC-1310 and HC-1550 fibers for telecom wavelengths [35] have dimensions typical for single-mode fibers (Table 1) but are unsuitable for telecom networks due to high attenuation: 60 dB/km @ 1310 nm, and 30 dB/km @ 1550 nm and propagation of higher-order modes.

Table 1. Technical data of NKT Photonics HC-1310 and HC-1550 PBGFs for telecom wavelengths and conventional single-mode fiber Corning SMF-28e+. Adapted with permission from Ref. [35], © NKT Photonics 2022, and Ref. [30], © Corning Inc., 2021.

Parameter	HC-1300	HC-1550	SMF-28e+
Core diameter (nom.) [μm]	10.0	11.5	8.2
Mode field diameter (nom.) [μm]	7.5 @ 1300 nm	9.0 @ 1550 nm	9.2 @ 1310 nm 10.4 @ 1550 nm
Cladding diameter (nom.) [μm]	125	120	125
Range of operating wavelengths [nm]	1290–1330	1490–1680	1260–1675
Attenuation (max.) [dB/km]	60 @ 1300 nm	30 @ 1550 nm	0.35 @ 1310 nm 0.20 @ 1550 nm
Attenuation (typ.) [dB/km]	30 @ 1300 nm	18.5 @ 1550 nm	0.18 @ 1550 nm
Chromatic dispersion (typ.) [ps/nm·km]	66 @ 1300 nm	42 @ 1550 nm	17 @ 1550 nm

Table 2. Data of single-mode fibers: OFS AccuCore (HC-PBGF) and Corning SMF-28e+ [30].

Parameter	AccuCore	SMF-28e+
Core diameter (nom.) [μm]	25.0	8.2
Core area (nom.) [μm^2]	491	52.8
Effective area, A_{eff} (nom.) [μm^2]	200	82
Ratio of A_{eff} to core area	0.41	1.55
Mode field diameter, MFD (nom.) [μm]	17.9 @ 1550 nm	10.4 @ 1550 nm
Cladding diameter (nom.) [μm]	82 [1]	125
Jacket diameter (see Section 7.1) [μm]	220 [1]	(125)
Effective refractive index, n_{eff} @ 1550 nm	1.005	1.468
Low-loss band [nm]	See Figure 4	1260–1675
Attenuation (max.) [dB/km]	7.0 @ 1550 nm	0.20 @ 1550 nm
Attenuation (typ.) [dB/km]	4.0 @ 1550 nm	0.18 @ 1550 nm
Chromatic dispersion (typ.) [ps/nm·km]	−70 @ 1550 nm [2]	17 @ 1550 nm
PMD [ps/$\sqrt{km}$]	9.15 [3]	≤0.10

[1] No data published by OFS—Estimate. [2] High dispersion at the edges of transmission band: −377 ps/nm·km @ 1545 nm [22]—see Figure 8. [3] Average value for spun fibers in a loose-tube cable [22].

OFS Fitel makes HC-PBGFs installed in commercial networks, mostly low-latency links for high speed trading, presented in Section 12.1.3. Selected data of OFS AccuCore fibers [21,22,27,28,34,36] are listed in Table 2.

HC-PBGF has three advantages over solid single-mode fibers:

- Low latency (−31.5% vs. SMF-28e+) [27,36];
- Low optical nonlinearity and ability to handle high optical power;
- Resistance to ionizing radiation.

As regards disadvantages, an important one is high PMD, resulting from the following factors:

- Lack of 90° rotational symmetry: eight shunts would be better (Section 7.2);
- Considerable distortions of fiber structure, especially the core (Figures 5b,c and 6).

PMD in similar un-spun HC-PBGFs was often in excess of 100 ps/$\sqrt{km}$, rising when the long-wavelength edge of transmission band was approached [23–25].

High PMD makes AccuCore fiber suited only for short links with NRZ coding (no added latency due to complex coding/decoding and FEC processing) operating at 10 Gb/s rate, which typically tolerate instantaneous differential group delay (DGD) of 30 ps, and a PMD of 10 ps—see Section 11. Because of radiation resistance and latency stability (see Section 7.3), similar fibers are also useful in nuclear facilities, space equipment, and multi-antenna microwave systems.

5. Fibers with Anti-Resonant Guidance

Such fibers share a common light guidance mechanism: anti-resonance in thin glass walls ("membranes") and slabs in Kagome fibers, or curved walls of tubes. This kind of hollow waveguide is known as anti-resonant reflecting optical waveguide (ARROW).

5.1. Optical Resonance and Anti-Resonance

Resonance condition means a light wave is reflected back into the slab at its surface and forward again, matching wave which did not experience reflections, and both waves propagate out of the slab without loss. This occurs when the phase delay in the glass wall/slab of thickness t and made of glass with a refractive index n is of 2πm, where m is an integer number (1, 2, 3,...), indicating how many times the reflected wave travelled back and forth across the thickness of slab. Assuming that the refractive index of filler gas is 1, this corresponds to a resonant wavelength λ_R [10,19] as follows:

$$\lambda_R = 2t\sqrt{(n^2 - 1)}/m, \quad (2)$$

and a resonance frequency f_R, as follows:

$$f_R = mc/2t\sqrt{(n^2 - 1)}. \quad (3)$$

The required wall thickness is calculated as follows:

$$t = m\lambda_R/2\sqrt{(n^2 - 1)}. \quad (4)$$

At resonance wavelengths, the wall or tube is transparent, and a waveguide surrounded by such structures experiences leakage; thus, the attenuation is very high. At anti-resonance, the phase shift is $(2m - 1)\pi$, the wave reflected back and forth is reversed in phase, and the interference with un-reflected wave is destructive—combined waves are weakened. At anti-resonance wavelengths, the waveguide exhibits the lowest confinement loss (CL). The anti-resonant wavelength λ_{AR} and wall thickness t are as follows:

$$\lambda_{AR} = 2t\sqrt{(n^2 - 1)}/(m - 0.5), \quad (5)$$

$$t = (m - 0.5)\lambda_{AR}/2\sqrt{(n^2 - 1)} \quad (6)$$

For λ_{AR} = 1550 nm and n = 1.4440 (fused silica), t = 0.582 μm for m = 1, and 1.746 μm for m = 2. Many fibers are designed with $m \geq 2$ for cladding robustness.

The spectra of both wavelengths are periodic and the low-loss band of the fiber (often called "window 1" for m = 1, "window 2" for m = 2, etc.) can be tuned by choosing the thickness of walls and number m. The diameter of tubes or spacing of walls (in Kagome fibers) has no effect on both wavelengths, but the leakage loss rises with it.

Each transmission window extending (theoretically) between the adjacent resonant frequencies f_{Rm} and f_{Rm+1} has the same bandwidth measured in the frequency domain, as follows:

$$\Delta f = c/2t\sqrt{(n^2 - 1)}. \quad (7)$$

In the wavelength domain, each subsequent window is narrower—see Figure 9.

For m = 1 and m = 2, the ratio of resonant wavelengths is 2:1, and a wide low-loss band is possible, unlike HC-PBGFs. The inclusion of additional tubes in nested or double nested nodeless anti-resonant fibers (NANF and DNANF) enables the designers to further extend the low-loss bandwidth by shifting the resonant (transparency) wavelengths of each tube.

Increasing m and/or λ_{AR} results in larger wall thickness, which makes fiber cladding less prone to distortions during drawing, but proportionally reduces fiber bandwidth and increases the overlap of optical power with glass, because walls are thicker, while the spaces between them remain similar. This increases fiber loss if the bulk loss of the fiber material is high, e.g., at $\lambda \geq 2100$ nm in the case of fused silica—see Figure 10 and Sections 6.1 and 6.2.

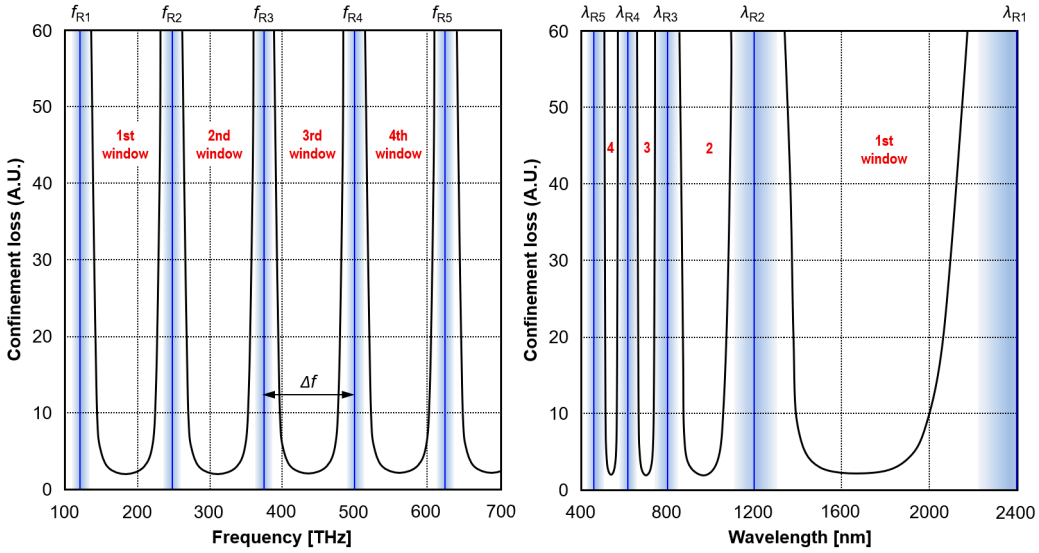


Figure 9. Example of arrangement of low-loss bands ("windows") in anti-resonant fiber, shown in frequency domain (**left**) and wavelength domain (**right**). High-loss bands between windows are centered around resonant wavelengths. Loss components other than CL not shown.

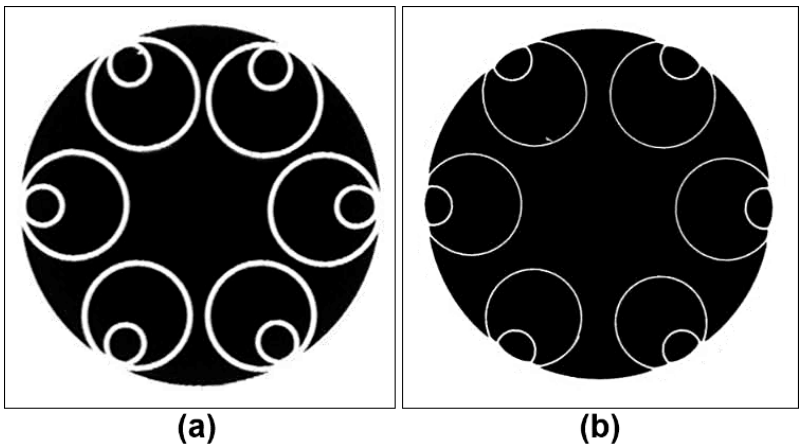


Figure 10. SEM images of core and cladding of six-tube NANFs: (**a**) m = 2, D_{core} = 31 µm, $\lambda_{AR} \approx$ 1450 nm, t = 1.17 µm, (**b**) m = 1, D_{core} = 35 µm, $\lambda_{AR} \approx$ 1550 nm, t = 0.415/0.46 µm (outer/inner tubes) [37–39]. Reproduced with permission.

A detailed analysis of light propagation in anti-resonant fibers can be found in [19]. Chromatic dispersion in NANF fibers was analyzed by Zeisberger et al. [40].

5.2. Kagome Fibers

Fibers of this type (Figure 2) feature three sets of flat, equally spaced walls intersecting at 60° angles (Figure 2a). Kagome fibers have been researched since 2002 [41], but achieving low loss and purely single-mode propagation proved difficult, partly due to scattering at numerous "nodes" or intersections of walls, as in HC-PBGFs [18]. It is also difficult to make a Kagome fiber with the desired flat walls intersecting at a 60° angle, as—unlike a hexagonal pattern in cladding of PBGF or round capillaries in NANF—such structures are not naturally created by or retained under the influence of surface tension when the fiber or "cane" is drawn. Figure 11 shows the extent of the deformation experienced in typical conditions.

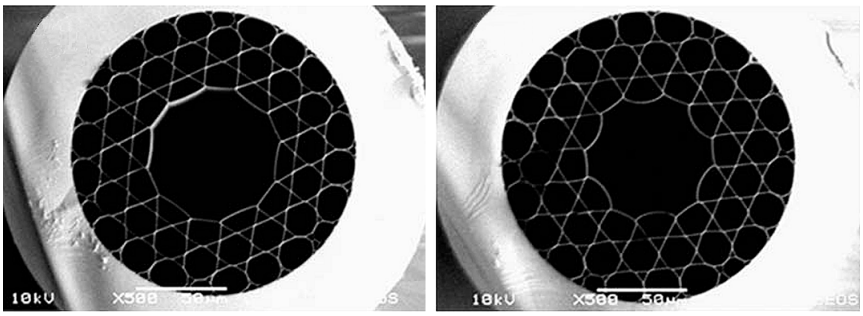


Figure 11. SEM images of Kagome fibers: (**a**) with round core; (**b**) with "hypocycloid" core delimited by round surfaces [42]. The white bar corresponds to 50 µm. Please compare with perfect structures shown in Figure 2a,b. Reproduced with permission.

The lowest loss reported in 2018 for Kagome fiber was 8.5 dB/km at 1080 nm [43]. Hybrid Kagome fibers with an added "negative curvature" layer of tubes or half-domes (Figure 2b,c and Figure 11b) were developed, exhibiting good single-modedness [44,45], and loss reduced to 1.6 dB/km at 1050 nm in 2021 [45]. However, the NANF and DNANF fibers presented in Section 5.3 have lower loss, down to 0.17 dB/km [13] and a wider bandwidth.

5.3. NANF and DNANF Fibers

The evolution of anti-resonant fibers was rather long. It began with Kagome fibers, presented in Sections 2.1 and 5.2, and was later followed by the introduction of round "negative curvature parts" surrounding the core for a lower overlap of optical power with glass. Once this approach was proven effective, the whole multi-layer Kagome cladding was replaced in 2011 with a single layer of tightly packed (touching) glass tubes or "capillaries" separating the empty core from the jacket tube [46]. This design was soon improved in 2013 [47] via the introduction of small gaps between the tubes, as shown in Figure 12a. The loss of this fiber at medium-infrared wavelengths was reduced substantially below bulk absorption in the glass.

A Nested Anti-resonant Nodeless Fiber (NANF) fiber was proposed by F. Poletti of the University of Southampton in 2014 [48]. In an NANF, the number of anti-resonant walls is doubled (Figure 12b), reducing confinement loss and allowing the designers to extend the low-loss bandwidth by differentiating the wall thickness and resonant wavelength of each tube. The lowest attenuation of NANF, reported in 2021, was 0.22 dB/km at 1625 nm [49]—comparable to the attenuation of commercial SMF [30] at the same wavelength.

Confinement loss can be further reduced via the inclusion of an additional small tube, resulting in Double Nested Anti-Resonant Nodeless Fiber (DNANF)(Figure 12c).

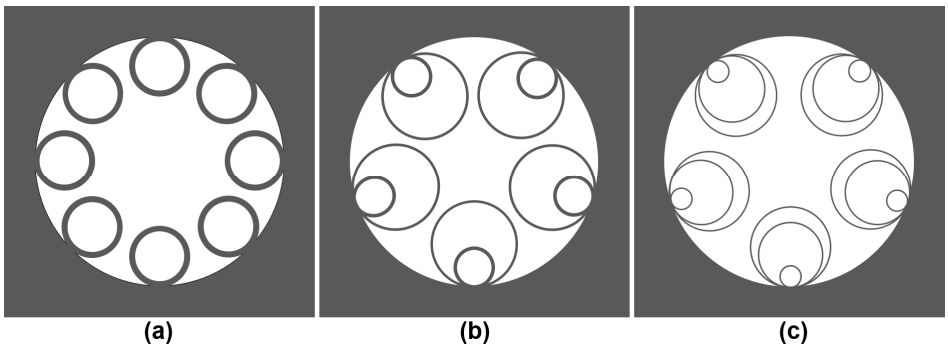


Figure 12. Main types of Anti-Resonant fibers: (**a**) with non-touching single tubes, (**b**) with nested tubes (NANF), (**c**) with double-nested tubes (DNANF). Fibers of type (**b**,**c**) had a minimum loss of 0.23 dB/km [49] and 0.174 dB/km [13], respectively. For an actual image of the last fiber, see Figure 13a.

This design was proposed and studied in 2014 by Belardi and Knight [50] and Poletti [48]. The reduction in confinement loss down to 10^{-5} dB/km was predicted using computer simulations, as each membrane added between the cavity and outer cladding ("jacket", see Section 7.1), preferably close to the core cavity, reduces the proportion of light propagating in the radial direction. In NANF and DNANF, nodes exist only between outer surfaces of tubes and the jacket tube, where the power density is very low. Light scattering is very low despite a considerable degree of fusion between the nested tubes and jacket observed in several fibers—see the example shown in Figure 13a. The lowest total loss so far, 0.174 dB/km at 1530 nm, was achieved in a DNANF in 2022 [13]. The photonic structure of this fiber is shown in Figure 13a, and the loss spectrum in Figure 14. Figure 13b is a comparison of the mode field distributions in this DNANF and equivalent NANF with an identical core diameter (28 μm). In a DNANF, the outer part of mode field is kept farther away from the fiber jacket by the relatively large middle tube and radial confinement loss reduced tenfold.

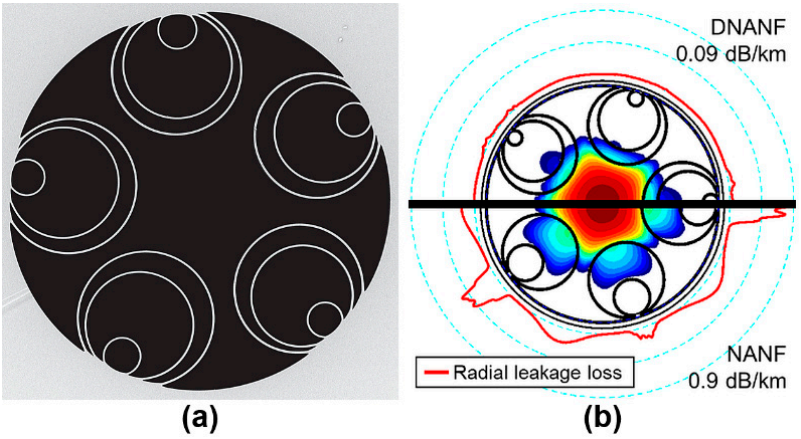


Figure 13. (**a**) SEM image of 0.174 dB/km DNANF, (**b**) simulated mode field distributions and radial confinement loss in this fiber and equivalent NANF [13]. Reproduced with permission.

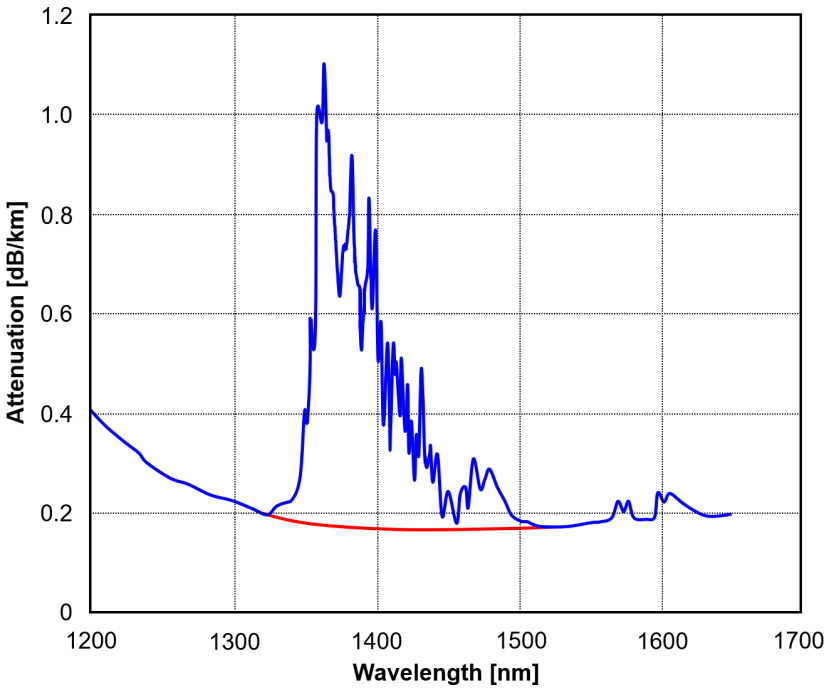


Figure 14. Loss spectra of lowest-loss DNANF fiber [13]: (blue) measured, (red) estimated for fiber without water peak.

With marginal loss contribution from bulk absorption in fused silica or other material, and proper scaling, NANFs can be optimized for different spectral ranges, including 850 nm and visible light, where a lower loss in comparison to solid fused silica multimode fibers was demonstrated [49]. The number of tubes is usually five, six or seven, sometimes eight or ten.

In addition to "basic" ARF/NANF/DNANF fibers with all round tubes shown in Figure 12, several other designs exhibiting a low (predicted) confinement loss were recently proposed, including NANF with elliptical inner tubes (Figure 15a, CL $\approx 10^{-3}$ dB/km) [51], DNANF with two parallel smallest tubes located in the same radial distance from the fiber axis (Figure 15b, CL $\approx 10^{-5}$ dB/km) [52], and ARF with non-nested stadium-shaped tubes elongated in the radial direction (Figure 15c) to increase the distance between the cavity and the outer jacket, and improve the azimuthal confinement of light [53].

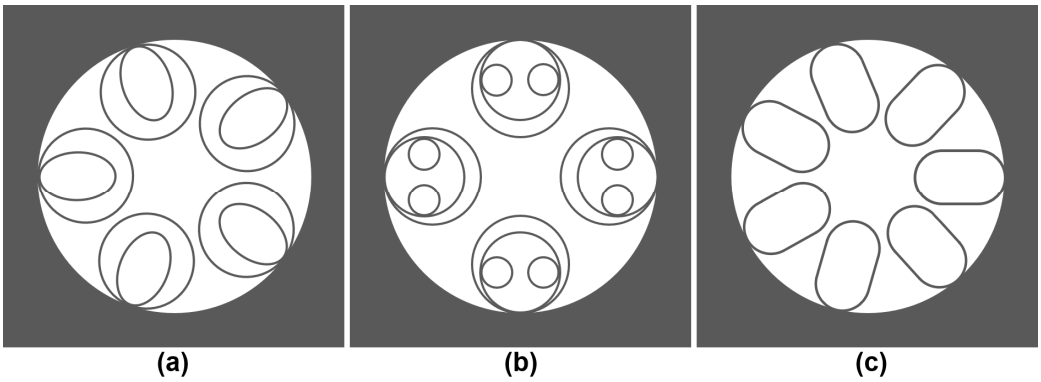


Figure 15. Alternative ARF structures with low confinement loss: (**a**) NANF with elliptical inner tubes [52], (**b**) DNANF with two parallel inner tubes [53], (**c**) ARF with "stadium" tubes [54].

Unfortunately, the substantial reduction in confinement loss alone cannot proportionately decrease the total fiber attenuation, as other loss components like SSL (Section 6.2), absorption by gas contaminants (Section 6.3), or bending loss remain.

The chromatic dispersion of NANF fibers designed for the 1550 nm band is low: 1.5–4 ps/nm·km (Figure 16), with flat characteristics over a wide range of the spectrum: 200 nm and more [12]. This property is valuable in long-distance DWDM systems, eliminating or substantially reducing the need for dispersion compensation.

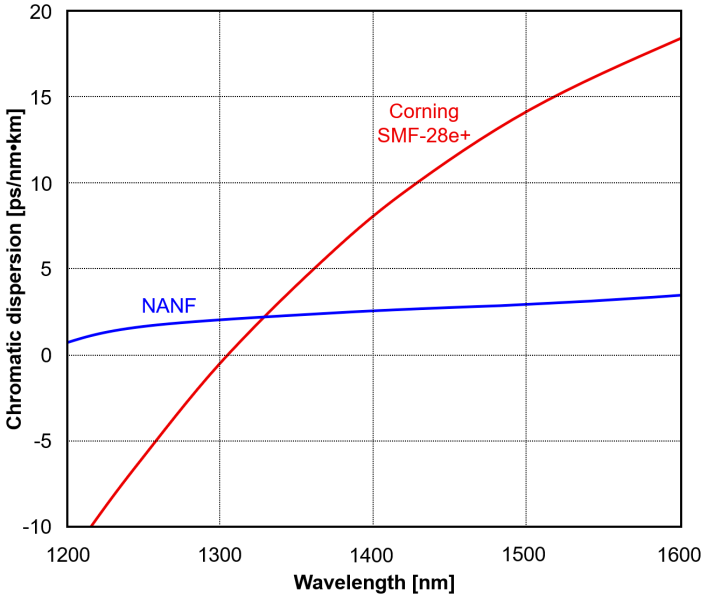


Figure 16. Chromatic dispersion of typical NANF [12] and Corning SMF-28e+ [30] fibers. In NANF, CD slope rises close to resonant wavelengths; negative CD at short wavelengths is possible [12,40].

Despite a lack of rotational symmetry of cladding, the PMD measured in 10 km of concatenated NANF fibers in a loose-tube duct cable was moderate: 0.29 ps/$\sqrt{}$km [54], close to the requirement for SMF, $\leq$0.20 ps/$\sqrt{}$km [29]. The reasons for this are explained in Section 7.2.

NANF cables are manufactured commercially under the trade name CoreSmart by a British company Lumenisity—a spinoff from the University of Southampton, acquired by Microsoft in December 2022, with a first deployment for HST connection to the London Stock Exchange in March 2021, and with installed lengths of up to 45 km. Table 3 is a comparison of Lumenisity CoreSmart NANF fiber to solid single-mode fiber. In the absence of published product specifications, data from research papers, primarily [12,13,49,54,55], were substituted and some parameters estimated.

Fused silica NANF with low loss, 0.85–1.25 dB/km in several bands close to 2 µm (≈1980 nm, ≈2040 nm, ≈2100 nm), was also reported by researchers from the Beijing University of Technology in China in 2021 [56]. This fiber was designed for optical power delivery, with a large core diameter (46 µm) and cladding made of five nested tubes.

Table 3. Comparison of single-mode fibers: NANF and Corning SMF-28e+ [30].

Parameter	NANF	SMF-28e+
Core diameter [µm]	29–36	8.2
Mode field diameter, MFD (nom.) [µm]	18–25 @ 1550 nm	10.4 @ 1550 nm
Cladding diameter (nom.) [µm]	82	125
Jacket diameter (see Section 7.1) [µm]	200	(125)
Effective refractive index, n_{eff} @ 1550 nm	1.003	1.468
Low-loss spectrum [nm]	1250–1650 [1]	1260–1675
Attenuation @ 1310 nm [dB/km]	0.22–0.40	$\leq$0.35
Attenuation @ 1550 nm [dB/km]	0.20–0.35	$\leq$0.20
Chromatic dispersion (typ.) [ps/nm·km]	1.5–4 @ 1550 nm	17 @ 1550 nm
PMD [ps/$\sqrt{}$km]	0.29	$\leq$0.10

[1] Limited by strong "water peak" (1.1–1.4 dB/km @1364 nm)—see Figure 14.

NANF/DNANF fibers are promising for communication networks, especially high-capacity DWDM networks. Advantages over solid single-mode fibers include the following:

- Low latency (−31,7% vs. SMF-28e+);
- Low and weakly wavelength-dependent chromatic dispersion;
- Low optical nonlinearity and ability to handle high optical power;
- Resistance to ionizing radiation.

Low-loss bandwidth and minimum attenuation are currently comparable, but:

- NANFs suffer from "water peak" absorption in the 1350–1490 nm band (Figure 14);
- The loss of NANFs can be further reduced [13], while that of solid-core fibers cannot.

Other disadvantages, applicable to all HCFs, include:

- Difficult splicing (Section 10);
- Sensitivity to contamination in adverse environments (Sections 6.3 and 6.4);
- Large, non-standardized diameter of most fibers (Section 7.1).

6. New Transmission Medium: Gas

6.1. New Properties of Fiber

The radiation guided in HCF interacts little with glass, as the photonic cladding consists predominantly (over 90%) of gas trapped between thin membranes or in tubes. This effect is quantified using an overlap of optical power distribution with glass parts to calculate the optical overlap coefficient (η). The ranges of values reported in literature are [4,5]:

- $\eta = 10^{-3}$–10^{-2} (0.1–1.0%, or 1000–10,000 ppm) for HC-PBGF fibers;
- $\eta = 10^{-5}$–3×10^{-4} (0.001–0.03%, or 10–300 ppm) for ARF fibers like NANF.

An increase in core diameter reduces η and fiber attenuation; therefore, HCF designers prefer large core diameters and mode field. The η coefficient is wavelength-dependent, rising at short wavelengths. Consequences of effective removal of glass from the transmission path are substantial:

- Loss can be, in theory, reduced to ≈0.001 dB/km [48,52]—see Section 6.2.
- Effective refractive index (n_{eff}) of fiber is low: ≈1.005 for HC-PBGF, ≈1.001 for NANF.
- Optical nonlinearities resulting from interaction with glass are reduced in proportion to optical overlap coefficient η multiplied by the ratio of effective core area (A_{eff}) of SMF and HCF, approx. 1:4. In a typical HC-PBGF, Kerr nonlinearity is ca. 500× lower than in SMF; for NANF, the difference is in the order of 1:10,000. In a fiber with very low η like NANF, the contribution of gas to nonlinear effects can dominate [5].
- Backscattering is mostly produced by surface scattering, which is quite strong in HC-PBGFs, almost absent in ARFs, and filler gas, and dominant in NANF/DNANF, but weak; the contribution of Rayleigh scattering in fused silica is marginal [57]. Backscattering in ARFs is very weak and the fiber can hardly be tested with OTDR—see Section 7.4.
- Chromatic dispersion (CD) and polarization mode dispersion (PMD) in HCFs are substantially different from such parameters of solid-core fibers, and very different for each kind of HCF—see Section 7.2 and Tables 2 and 3.
- Splicing and termination techniques must ensure hermetic sealing to prevent fiber contamination, e.g., with water vapor—see Sections 6.3 and 6.4.
- Contaminated fiber can be purged with pure gas, but this can take several days for a 1 km long fiber with 100 µm core at 100 kPa overpressure [58]—See Section 6.4.
- HCFs exhibit much better stability of latency than solid-core fibers when subjected to variable temperatures, but not strain—see Section 7.3.
- HCFs are resistant to ionizing radiation, as color centers and associated bulk absorption in fused silica have little effect on fiber attenuation [59]. However, radiation can deteriorate fiber coatings and the polymer parts of the cable.

6.2. Origins of Fiber Loss

The attenuation in HCF is produced via several mechanisms:

(a) Escape of light through cladding, causing confinement loss (CL);
(b) Surface scattering loss (SSL) [11];
(c) Absorption by contaminants of filler gas, e.g., water vapor (Section 6.3);
(d) Absorption of bulk silica glass, important at long wavelengths [26];
(e) Micro- and macrobending loss;
(f) Loss resulting from structural imperfections of photonic cladding [60].

Each loss component is wavelength-dependent in a different way. Loss analysis for NANFs is presented in [19,61], and for HC-PBGF in [26].

CL is used to measure how effectively the cladding blocks escape of guided light from the fiber's core at a particular wavelength. It depends both on cladding design and the accuracy of controlling its geometry during fiber manufacturing. CL is also known as "Leakage Loss".

CL can be, in theory, reduced as desired via the modification of cladding, e.g., adding layers of holes or nested tubes, with predicted values in DNANF fibers down to $\approx 10^{-5}$ dB/km [48,52]. However, manufacturing imperfections and variations in key dimensions have a considerable influence [60]. For example, the thickness of walls around the core of HC-PBGF shall be a half of the thickness of the struts to minimize the attenuation.

SSL is produced by thermally excited Surface Capillary Waves (SCW) in molten glass, which is frozen when the fiber is cooled after drawing. Light guided in the fiber is scattered on uneven surfaces encircling the hollow core; the resulting attenuation in HC-PBGF is proportional to λ^{-3} [11]. Recent analyses and experiments [62] indicate that the application of surface shear during fiber drawing can reduce the RMS height of SCW from ≈0.4 nm in fibers drawn without shear to ≈0.15 nm at most important SCW wavelengths

shorter than 1 μm, with an expected threefold reduction in SSL. Surface scattering is partly backscattering, beneficial for fiber measurement with OTDR.

SSL is decreased by increasing the core diameter to minimize the overlap of guided light with glass surfaces around the fiber's core, and is negligible in NANF/DNANF fibers.

With adequately low η, HCF can have low attenuation despite a high loss of fused silica or other structural material. In particular, an effective onset of phonon absorption in SiO_2 fiber is shifted from 1500 nm in SMF to 1800–2200 nm [26]. In an HC-PBGF with η = 0.5%, the minimum loss of leakage-free hollow-core fiber, limited by phonon absorption in fused silica, can be as low as 0.01 dB/km at 1800 nm, rising to 1 dB/km only at 2150 nm [11,20]. For an NANF with η = 0.01% (100 ppm), the minimum loss produced by phonon absorption in glass is below 0.001 dB/km at wavelengths close to 2000 nm.

Loss resulting from Rayleigh scattering in glass is not important in HCFs because its value in bulk glass (≈0.14 dB/km @ 1550 nm) is multiplied by η—more at long than at short wavelengths. This enabled the development of NANFs operating at visible wavelengths, with a loss lower than that in solid-core fused silica fibers, e.g., 2.8 dB/km at 660 nm [63].

The same applies to hollow-core polymer optical fiber (HC-POF). Solid POFs have a core of PMMA and thin cladding of fluorinated polymer. These fibers have too high attenuation for telecom networks, 150–200 dB/km at 650 nm, and 80–100 dB/km at 480 nm and 520 nm [64], and are restricted to short data links in vehicles, industrial automation, etc. The attenuation of PMMA HCF with $\eta \leq 0.005$ can be, in theory, reduced to ≤1 dB/km in the 600–850 nm band [65]. This is less than the typical attenuation of OM2/3/4/5 multimode solid-core fibers used in LANs and data centers: 2 dB/km at 850 nm [66].

The attenuation of state-of-the art fused silica HC-PBGF is primarily a sum of:

- CL, which usually reaches high values in several bands, usually leaving narrow low-loss transmission band(s) (Figure 4).
- SSL, which imposes a low limit of fiber loss at short and medium wavelengths, up to 1800–1900 nm, where the associated loss can fall down to 0.1–0.2 dB/km [26] in optimized fibers, but is much higher, ≈2 dB/km in current commercial HC-PBGFs.
- Bulk absorption in fused silica, multiplied by the optical overlap coefficient η. Due to low η, bulk absorption is important only at wavelengths above 1800 nm [26].

In a state-of-the-art NANF/DNANF, the largest components of attenuation are:

- CL, with minima at anti-resonant wavelengths and rising closer to resonant wavelengths [48,52]. This splits the low-loss spectrum into multiple "windows" (Figure 9). CL can be very low, down to 10^{-5} dB/km [48,50,52], but other loss components are larger.
- SSL, ≈0.03–0.05 dB/km at wavelengths in the 1500–1800 nm range [61], less than in HC-PBGFs due to lower power density at surfaces of cladding tubes.
- Absorption by contaminants of filler gas (Section 6.3).
- Microbending loss.
- Loss resulting from structural imperfections of cladding like variations in capillary diameters (Section 9) or their excessive fusion with fiber jacket.

Loss due to bulk absorption in fused silica, multiplied by η, is below 0.01 dB/km in typical NANF/DNANF at wavelengths up to 2200 nm of interest in telecom networks [61].

Microbending loss in a typical NANF:

- Falls with an increase in wavelength [38,61]—in SMF, the situation is opposite;
- Rises with an increase in core diameter and MFD—as in SMF.

It is the rising microbending loss that imposes a practical limit on the NANF/DNANF core diameter, approx. 40 μm. The minimum predicted total attenuation of optimized and flawless DNANF of current design is around 0.055 dB/km at 1550 nm [61].

6.3. Absorption and Scattering by Filler Gas and Contaminants

Because 99–99.999% of radiation propagating in HCF interacts with gas filling the core rather than material of which the photonic structure is made, ensuring low attenuation

depends on the properties and the purity of this gas, including absorption by gas, its impurities and deposits on surfaces around the core, as well as Rayleigh scattering.

The advantages of gas over glass or polymer include a low refractive index, ≈1.000273 at 1550 nm for air at room temperature and standard atmospheric pressure at sea level [67], and very weak Kerr, Raman and Brillouin effects at atmospheric or lower pressure.

Unfortunately, filling gas can be contaminated with species:

- Present in the working area of the fiber manufacturing plant: water vapor, carbon dioxide, or fuel for gas burners;
- Out-gassing from hot glass, mostly chlorine and fluorine present in commercial fused silica tubes in concentrations up to 2000 ppm, and 3200 ppm for Heraeus F300 and F320-08, respectively [68];
- Diffusing into the fiber through open ends and imperfectly sealed splices, like hydrogen, water vapor, and methane [69,70].

Argon is used as protective gas during fiber drawing to prevent the burning and oxidation of oven parts, and is also suitable as filler. In most experiments, purified air is used.

Attenuation produced by Rayleigh scattering in a dry, dust-free air or pure argon at 101.3 kPa pressure (standard atmospheric pressure at sea level) is approx. 0.035 dB/km at 600 nm and 0.14 dB/km at 400 nm, respectively, if a complete loss of scattered light is assumed [71,72]. This attenuation is proportional to the effective cross-section of Rayleigh scattering of a particular gas and its pressure.

While helium has the lowest cross-section of Rayleigh scattering—Ca. 60× lower than air [72]—and few absorption lines in the spectral range of interest (Table 4), this gas can easily diffuse out from fiber or splice, and appears unsuitable.

Table 4. The strongest absorption lines or bands in non-ionized state between 600 nm and 2200 nm, and Rayleigh scattering cross-sections [σ] at 733 nm, of possible filler gases and their contaminants [72–76]. Notes: (1) absorption bands are usually composed of numerous narrow absorption lines; (2) limits of bands correspond to approx. 10% of peak absorbance.

Gas	σ [10^{-32} m^2]	Absorption Lines or Bands [1] [nm]
Helium (^{4}He)	0.39	668, 707, 1083, 2058
Argon (Ar)	23.8	697, 707, 750, 764, 795, 801, 810, 812, 912, 966
Nitrogen (N_2)	26.5	744, 747, 868, 1247, 1358, 2099–2206
Oxygen (O_2)	22.0	777, 845, 927, 1253–1283
Chlorine (Cl_2)	no data	822, 838, 859
Fluorine (F_2)	no data	686, 704, 713
Hydrogen (H_2)	5.30	656, 1282, 1875
Methane (CH_4)	59.2	1631–1679
Propane (C_3H_8)	346	1685–1765
Ammonia (NH_3)	38.9	1471–1547, 1926–2025, 2200–2348
Water vapor (H_2O)	19.2	1117–1153, 1352–1414, 1816–1934
Carbon dioxide (CO_2)	62.2	1432, 1438, 1998–2026

[1] All absorption lines are relatively weak.

The attenuation of HCF is increased by the absorption of gas and its contaminants. In particular, water is deposited on the inner surfaces and reacts with fused silica, producing silanol (SiOH) absorbing light at 1364 nm, while the initial concentration of water vapor decreases with time. Non-polar gases like nitrogen, oxygen or argon do not attach to fused silica surfaces [69].

The absorption lines (for elements) and bands (for compounds), and Raman scattering cross-section (σ) characterizing the intensity of Raman scattering are listed in Table 4. Only the strongest absorption lines or bands for each gas are listed. Data were compiled from the NIST Basic Atomic Spectroscopic Data for elements website [73], HITRAN on the Web website [74] and papers [75,76] for compounds.

The measurement of fiber loss spectrum enables the detection of contaminants and estimation of their average concentration, as the attenuation they produce is proportional to partial pressure. For example, the spectral loss graph of NANF published by Jasion et al. [55] reveals absorption bands of water vapor, ammonia, methane, propane and possibly one or two more compounds the authors failed to identify.

6.4. Exchange of Gases with Atmosphere and Entry of Water

Water vapor absorption is prominent in the spectral loss of the lowest-loss HCF reported so far [13], as shown in Figure 14. The water peak was 90 nm wide at an added loss of ≥0.2 dB/km, and 110 nm at ≥0.05 dB/km—the latter value is typical for conventional single-mode fibers conforming to the ITU-T G.652.D standard [29]. The shape of loss peak corresponds exactly to the absorption by water vapor in air [76].

Researchers from the University of Southampton have recently (2022) measured the dynamics of gas exchange between un-sealed lengths of HC-PBGF and NANF fibers and the surrounding atmosphere, absorption and Raman (Stokes) spectra of contaminants inside fibers, the internal pressure of gas in a freshly drawn NANF, and the infiltration of liquid water into a vertically suspended HC-PBGF [69,70]. Some findings are surprising, and important for the handling, splicing and repairs of HCFs and cables with them, as follows:

- The inner pressure in a freshly drawn fiber is 20–29 kPa, only 1/4th of the atmospheric pressure, despite the application of 6 kPa overpressure during drawing. This happened because the gas inside the preform was initially hot, ≈1400 °C during necking, and the pressure fell during cooling to room temperature, roughly by a factor of 5.7;
- The time required for the equalization of pressure inside a 55 m length of freshly drawn HC-PBGF with a 31.6 µm core diameter open at both ends with a surrounding atmosphere was 2 h. For a 34 m long 7-tube NANF with a smaller core diameter (18.5 µm), this time was longer—3 h;
- When a freshly drawn HC-PBGF (kept sealed after drawing, and cleaved 3 min before experiment) was vertically suspended, with one end sealed and the other immersed in pure water, the water column inside the fiber reached a height of 8.8 m after 40 h. For a pressure-equalized fiber, the result was still 2.1 m, as the water was driven into fiber by surface tension. The fiber tested was 26.5 m long.

In another experiment, the added spectral loss in HC-PBGF and five-tube NANF fibers was monitored, when a 150 m and 155 m length of each fiber were kept with one end open in the lab, at a controlled 40% relative humidity and 22 °C temperature for 10 months [70]. Then loss of NANF was stable throughout the test, while HC-PBGF exhibited an increase in loss of up to 10 dB at 1364 nm (SiOH absorption peak), and rising "water (vapor) peak" similar to the one shown in Figure 14. Fibers of the same type tested with fusion spliced SMF pigtails at both ends, and therefore sealed, exhibited stable loss for 3 months.

The difference is explained by a dramatic, roughly 250:1, difference between the overlap of optical power distribution with glass parts in each fiber: 0.5–1.0% in HC-PBGF, and only 0.002–0.005% (30–50 ppm) in low-loss NANF. The added attenuation was about 24 dB lower in NANF for an identical concentration of water vapor inside.

6.5. Chromatic Dispersion of Gas

The contribution of gas to chromatic dispersion of hollow-core fiber is negligible. For example, the material dispersion of argon at atmospheric pressure and room temperature [40] is approximately −0.048 ps/nm·km @ 850 nm, −0.012 ps/nm·km @ 1310 nm and −0.009 ps/nm·km @ 1550 nm. For comparison, the tolerances of a chromatic dispersion in a solid single-mode fibers allowed in IEC and ITU-T standards [29,77–79] are up to ±3 ps/nm·km.

7. Selected Properties of HCFs

In this section we present the following unique properties of hollow-core fibers important for some telecom, datacom, and similar applications, but not described before:

dimensions and their definitions (Section 7.1), polarization mode dispersion (Section 7.2), temperature and strain dependence of latency (Section 7.3), and backscattering (Section 7.4).

7.1. Fiber Dimensions

The cladding of solid-core optical fiber performs two functions: prevents the escape of light from the core and provides the tensile strength and rigidity of the fiber. To perform the first function in single-mode fiber operating at 1550 nm, cladding must have a minimum thickness (measured from the border with core) of 24–35 µm, depending on the presence of a "trench" structure around the core; otherwise, an increase in fiber attenuation resulting from light leakage, and rising exponentially with wavelength, occurs [80].

In hollow-core fibers, "cladding" means a photonic structure performing function (a). Its mechanical strength is marginal due to the small cross-section of glass parts. Mechanical strength and hermeticity are provided by a separate layer of solid glass, called "jacket" (Figure 17). In NANF or DNANF, the core diameter is the diameter of the largest circle fitting in the space between the tubes (Figure 17b).

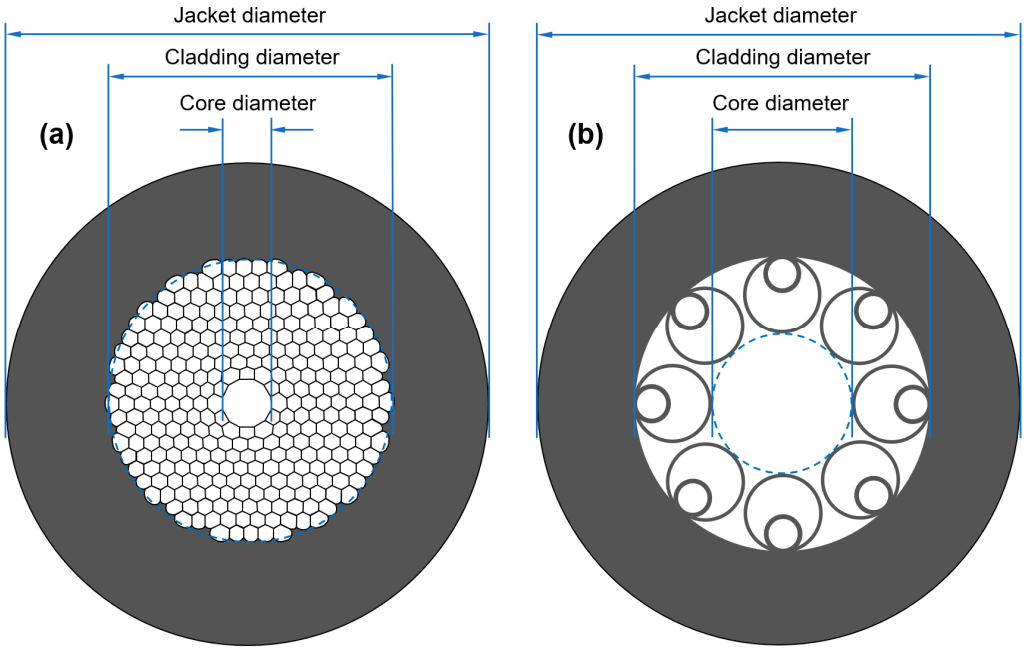


Figure 17. Main dimensions of hollow-core fibers: (**a**) HC-PBGF, (**b**) NANF.

The diameters of cladding in HCFs designed for transmission in the 1550 nm band are between 55 µm and 100 µm. If the HCF is to have tensile strength equal to solid 125 µm telecom fiber made of the same material, the cross-section of its jacket shall equal the total cross-section of telecom fiber: 12,272 μm^2.

Estimated cladding diameters of OFS HC-PBGF fibers presented in Section 4.2 and Section 4.3 and Lumenisity NANF and DNANF fibers presented in Section 5.3 are 82 µm and 90 µm, respectively. For tensile strength equivalent to that of a 125 µm solid-core fiber, jacket diameters of 150 µm and 154 µm are required, but the diameters estimated from photographs and drawings are larger: 220 µm and 200 µm. The authors suspect that a thick jacket of preform reduces the deformations of the cladding, especially its outer parts, caused by surface tension in softened glass during drawing.

7.2. Polarization Mode Dispersion

This parameter is important in telecom fibers for transmission at very high rates and over long distances. While fiber dispersion can be digitally compensated, this introduces latency due to signal buffering and processing, and is avoided in low-latency links.

PMD in solid single-mode fibers can be reduced by the spinning of hot fiber during drawing, introducing permanent rotation and the periodic reversal of orientation of locally added components of a differential group delay (DGD), thus preventing the accumulation of DGD along the fiber. Fiber spinning was developed in 1981 for sensor fibers [81], and introduced to telecom fibers in 1994 [82,83].

In HC-PBGF (Figure 4), one source of PMD is the non-circularity of the central cavity, probably due to the distortion of the preform during consolidation. High PMD observed in OFS AccuCore fibers (see Sections 4.2 and 4.3) is partly created by the deliberate introduction of a small non-symmetry of the core—ellipticity and local increase in wall thickness, to eliminate high-order modes at the expense of increasing PMD and PDL [32]. The PMD value for this fiber listed in Table 2 applies to fiber spun during drawing at a high rate of approx. 100 rev/m, corresponding to a spin period of 10 mm, and placed in an underground cable of a loose-tube design. PMD in un-spun fiber in the same conditions was $\approx$55 ps/$\sqrt{}$km, but micro- and macro-bending experienced by the fiber on a 150 mm diameter spool reduced it to $\leq$3 ps/$\sqrt{}$km—more effectively than spinning [21,22]. This behavior of HC-PBGF may spur the development of cables ensuring similar conditions for fibers inside.

PMD in NANF/DNANF results mostly from the ellipticity of the core, as in conventional single-mode fibers, but another source of PMD exists. Single-mode NANFs with a number of regularly spaced anti-resonant tubes exhibit some degree of "spill" of mode field into gaps between the tubes (Figure 18) as "spikes". If these spikes are not arranged with a 90° rotational symmetry, one state of polarization will experience transmission latency different from that of the orthogonal state, resulting in DGD. In typical NANF designs with 5–8 tubes (nested or not), one with 8 tubes exhibits 90° rotational symmetry, while one with 6 tubes exhibits the largest asymmetry (Figure 19). In fibers with five and seven tubes, the difference in propagation conditions between orthogonal polarizations is considerably lower.

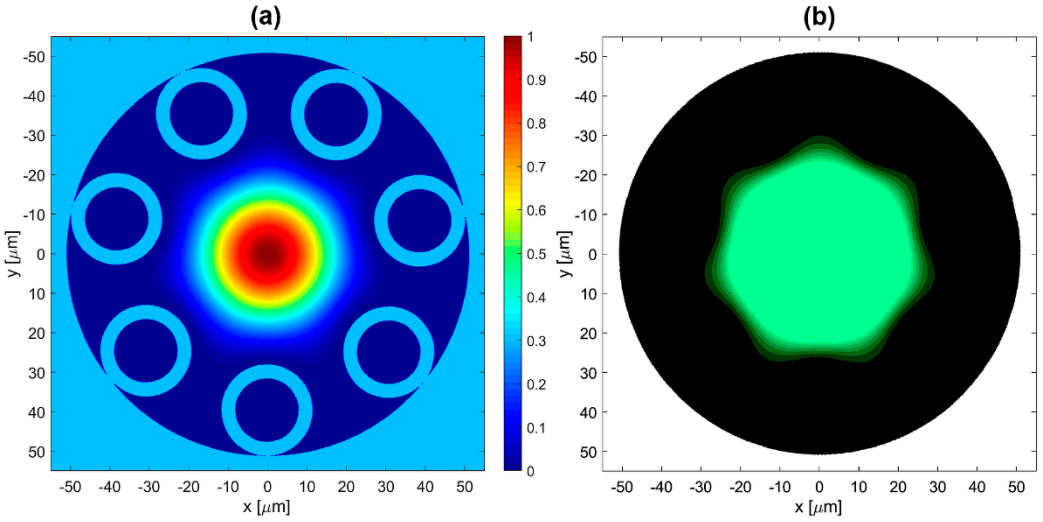


Figure 18. Distribution of power density in non-symmetrical NANF with seven tubes for 2 μm band: (**a**) false color image, (**b**) image adjusted to enhance peripheral parts of guided mode at 2 μm.

An NANF fiber has a structure with 90° rotational symmetry, incorporating eight tubes shall exhibit lower PMD than fibers with five, seven and, in particular, six tubes (Figure 19).

However, this mechanism of DGD creation is weak due to the following factors:

- Minimal interaction of optical power with tubes—only 0.001–0.03% of it is propagating in the glass, or other solid material the fiber is made of;
- Small angle between the directions of adjacent extreme field distributions [84]: 36°, 30°, 25.7° and 22.5° in an NANF with five, six, seven and eight tubes, respectively.

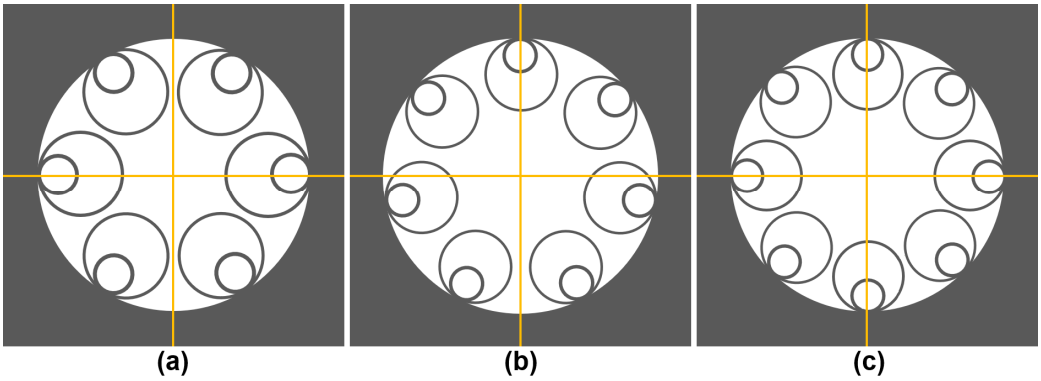


Figure 19. The 90° rotational (**a**) symmetry in NANFs: (**a**) un-symmetrical fiber with six nested tubes, (**b**) less un-symmetrical fiber with seven nested tubes; (**c**) symmetrical fiber with eight nested tubes. Yellow lines indicate orthogonal polarizations of light.

PMD measured in loose-tube duct cables with Lumenisity NANF fibers was quite low, 0.29 ps/$\sqrt{}$km, and transmission experiments at 400 Gb/s (95 Gbaud) rate and over distances up to 1128 km performed at BT laboratories were successful [54].

The distortion of mode field increases the loss of splice to conventional single-mode fiber with a circular mode field, e.g., by 0.08 dB for an NANF with six tubes (Figure 19a) [84].

7.3. Latency vs. Temperature and Strain

The latency of conventional single-mode solid-core fused silica optical fiber is affected by temperature, due to the thermo-optic coefficient of glass and fiber expansion as well as the tensile strain in the fiber. Both effects are strongest in aerial cables subjected to a wide range of temperatures (e.g., −40. . .+70 °C), vibrations, and variable tensile loads from wind or ice. Fiber optic cables in front haul links at radio sites are predominantly installed on masts or other structures exposed to the elements and solar radiation.

The common solid SMF conforming to ITU-T Recommendation G.652 [29] shows a linear increase in latency with temperature; the temperature coefficient of latency is ≈37.4 ps/km·K at 1550 nm for Corning SMF-28e+ fiber [30]. The same parameter for an HC-PBGF with 29.2 µm core diameter and 21.4 µm MFD was 2.0 ps/km·K [85].

Variations in latency have two sources. One is the increase in fused silica's refractive index with temperature, $11{\cdot}10^{-6}$/K, producing a latency change of ≈35 ps/km·K. The second is the change in fiber length with temperature: $\approx 0.55{\cdot}10^{-6}$/K for bare fiber and $\approx 2.0{\cdot}10^{-6}$/K for fiber in 250 µm primary coating. Due to the decrease in the glass refractive index with strain (elasto-optic effect), the relative change of latency is approx. 80% of the applied strain: $\approx 0.44{\cdot}10^{-6}$/K (≈1.4 ps/km·K) for bare fiber and $\approx 1.6{\cdot}10^{-6}$/K (≈5 ps/km·K) for primary coated fiber found in a typical loose-tube cable.

Only the second mechanism of latency variations is observed in HCF, as the gas inside has negligible variations in the refractive index with temperature and pressure. Typically, only 0.003% (30 ppm) of light in NANF propagates in glass [85], and there is almost no change in the effective refractive index with fiber strain; latency changes almost exactly in proportion to fiber length. The calculated temperature coefficient of HCF is $\approx 0.55{\cdot}10^{-6}$/K (≈1.75 ps/km·K) for bare fiber and $\approx 2.0{\cdot}10^{-6}$/K (≈6.4 ps/km·K) for fiber in primary coating, if the glass/polymer cross-section ratio is identical to one in SMF. The low value reported by Slavik et al. [84] was measured for a fiber in a thin coating, e.g., 10 µm thick.

Due to the reasons stated above, SMF subjected to tensile strain exhibits a 20–25% smaller variation in latency compared to HCF, whose latency is directly proportional to physical length.

When both SMF and PCF are encased in similar primary coatings made of dual layer epoxy-acrylate materials, the latency in HCF will be approx. 6 times less sensitive to temperature (18 times with thin coating), but approx. 1.25:1 more sensitive to tensile strain. For stable latency, a good protection of HCF against strain and thin coating is desired.

The measurements and modeling of comparative sensitivity of transmission delay to temperature in SMF-28 and fused silica PBGFs (Blaze Photonics HC-1550-02 and Crystal Fibre AIR-10-1550), all in typical acrylate primary coatings with outer diameters of 250 µm, 220 µm and 270 µm, respectively, revealed similar difference, approx. 4:1 and 5:1 [86]. This indicates that the sensitivity of the delay to temperature reflects the longitudinal expansion of HCF in a particular coating, regardless of the type of photonic cladding.

7.4. Backscattering

Light propagating in glass or gas, but not in a vacuum, is subject to scattering due to the microscopic non-uniformity of the bulk material—the omni-directional Rayleigh scattering produced by random non-uniformities much smaller than the wavelength (their dimensions in fused silica are in order of 0.2 nm), or scattering resulting from the thermally generated surface capillary waves "frozen" after drawing of HCF (see Section 6.2). The scattering cross-sections of gases is listed in Table 4. In a contaminated HCF, additional scattering may by produced by particles of dust, droplets of condensed vapor, or product(s) of its reaction with silica, deposited on surfaces around core. It may be a Mie scattering, as such particles have sizes comparable to the wavelength of light.

In solid-core optical fibers, only Rayleigh scattering in fused silica (usually doped) is observed, and this is the mechanism imposing a low limit on fiber attenuation at wavelengths up to 1550 nm. A small part of scattered radiation reflected backwards is captured by the fiber (ca. 0.12% in SMF, and 0.5% in 50/125 µm MMF) and propagated back to the light source. Backscattering is detrimental, producing interference in bidirectional data transmission, noise in analog TV links, feedback and instability in optical amplifiers, or complicating the monitoring and compensation of fiber latency (Section 12.2.1). On the other hand, backscattering enables researchers to measure fiber attenuation, non-uniformities and length with optical time domain reflectometer (OTDR). Without backscattering, OTDR would only be able to detect and locate fiber ends, splices and defects.

The lowest level of backscattering in SMF is approximately −76 dB/m at 1550 nm for fibers with pure silica core, and about −72 dB/m for typical SMF with a germania (GeO_2)-doped core. In an NANF, backscattering from fused silica parts of the fiber at the same wavelength is very low, about −115 dB/m [48,87], because only 0.001–0.03% of light interacts with glass parts of the fiber and the fiber acceptance angle is smaller than in SMF (NA = 0.02–0.03 vs. ≈0.14). With backscattering intensity ca. 40 dB lower, OTDR measurements of NANFs would be almost impossible, as this difference nullifies the OTDR dynamic range available at ≤20 m resolution: 15–25 dB one-way, or 30–50 dB of intensity difference.

The situation is changed by the gas in the core. In a typical NANF filled with dry air at a normal atmospheric pressure, the intensity of backscattering is approx. −100 dB/m, ca. 25 dB below that in a typical SMF [87], just enough to allow for OTDR measurements in NANF fibers of medium lengths, e.g., 10 km. The Doppler effect in air at room temperature causes the spectral widening of backscattered light by some 500 MHz [88]. This broadening does not affect ordinary OTDR with a receiver responding to the intensity of the returning light, but OFDR with a narrowband receiver fails to detect the backscattering from gas.

As presented in Section 6.3, the type and pressure of filler gas affect the intensity of backscattering in an NANF. Vacuum NANF would produce almost no backscattering, being perfect for bidirectional transmission, but very difficult to test with OTDR.

In HC-PBGF, scattering at surface capillary waves, negligible in NANF, dominates (Section 6.2). In a fiber with small, "7-cell" core, e.g., NKT Photonics HC-1550 (Figure 4, Table 1), backscattering is quite strong, with approximately -77 dB/m estimated for a perfect fiber, and -60 dB/m measured in real fibers [87]. When the core is larger, ≈30 µm diameter or "19-cell" size, scattering is weaker, but still allows for measurements with typical OTDR [89].

8. Theoretical Analysis and Simulations of Hollow-Core Fibers

8.1. Models

Anti-resonant hollow-core fibers (AR-HCFs) are cylindrical waveguides in which the refractive index of the core is smaller than that of the surrounding cladding. Thus, the propagation mechanism of keeping the mode field in the fiber's core cannot be explained by the total internal reflection (TIR) phenomenon as in conventional step-index single-mode fibers. On the other hand, what distinguishes AR-HCFs from HC-PBGFs is that the former do not have a periodic cladding, which determines the existence of a photonic band gap that traps the propagating light in the core. Thus, considering the guiding mechanism, the AR-HCF fiber can be treated as a kind of leaky mode HCF.

Over the years, much effort has been put into developing models that can explain the propagation mechanism in leaky mode HCF fibers. The most commonly used are the Marcatilli and Schmeltzer model, the anti-resonant reflecting optical waveguide (ARROW) model and the coupled mode model.

In 1964, Marcatilli and Schmeltzer published the pioneering analytical studies on the mode properties of a circular hollow-core dielectric waveguide. In their model, the air-filled core was surrounded by infinite homogenous absorption-free cladding of a higher refractive index. In this structure, regardless of the incident angle, only the partial reflection occurs at the boundary between the core and the cladding. Thus, the fraction of optical power radiates into the cladding, which causes the mode attenuation. The imaginary part of derived propagation constant γ represents the loss coefficient of the analyzed structure and is given by the following formula [90]:

$$\alpha_{nm} = \mathrm{Im}(\gamma) = (u_{lm}/2\pi)^2 \cdot (\lambda^2/r^3) \cdot \mathrm{Re}(\nu_l) \quad (8)$$

where u_{lm} is the m-the zero of the Bessel function $J_{l-1}(u_{lm})$, l, and m are radial and azimuthal number of modes, λ is wavelength, n and r are core refractive index and radius, respectively, and ν_l is the constant for different (TE, TM and EH) modes that depends on the refractive index of the cladding material. Using the Marcatilli and Schmeltzer model, it is also possible to calculate the bending loss according to the following formula [91]:

$$\alpha_{nm}(R) = (r^3/\lambda^2 R^2) \cdot \mathrm{Re}(\nu_{lm}) \quad (9)$$

where R is the bending radius and ν_{lm} is mode dependent constant. It is worth noting the limiting usefulness of the above model when real a AR-HCF fiber is analyzed. Formula (6) does not consider the multiple reflections of leaky modes on a complex cladding structure, which also affects the fiber mode attenuation. Moreover, the model does not support an analysis of the cladding modes.

In order to explain the mentioned multiple reflections, an anti-resonant reflecting optical waveguide (ARROW) [91] was proposed and was successfully verified to analyze the light transmission in HCF [92]. In this model, the analytical formulas for resonant wavelengths (2) and anti-resonant wavelengths (3) are given and allow for the determination of the spectral bands where mode leakage is enhanced and where the propagating light is well confined in the core area, respectively. The multiband structure is similar to that obtained for the transmission spectrum in Fabry–Perot resonators. The ARROW model is based on the ray-optics approach, and the transmission bands can thus be accurately predicted when the $t >> \lambda$ condition is satisfied.

To consider the energy transfer between the core and the cladding modes, the coupled mode model was proposed. If the finite complex structure of the fiber cladding is assumed, then that high loss spectral regions result from the coupling between core (airy) modes and dielectric modes. This approach was used and numerically validated by Vincetti and Setti [93]. Numerical results show that the coupled mode model is able to analyze the loss and dispersion properties of the HCF, and enables a better understanding of the influence of fiber geometry on the propagation properties of the waveguide.

8.2. Simulation Tools

In recent years, most of the numerical analysis of guidance mechanism of AR-HCF has been based on full-vector finite element method (FEM) using the commercial software COMSOL Multiphysics. Alternative tools are FEM-based Femlab [46,47] and finite difference eigenmode (FDE) solver-Lumerical® MODE Solutions [65]. In order to efficiently and accurately simulate HCFs using the FEM model, it is important to carefully optimize both computational mesh, particularly sizes of finite elements, and a perfectly matched layer (PML)—an artificial, non-reflective and totally absorbing layer, allowing for the truncation of computational regions while simulating the propagation in HCF with a transparent jacket.

The mentioned solvers enable the calculation of the mode field distribution of individual fiber modes, their propagation losses—including higher-order mode extinction ratio (HOMER)—the measure of the single-modedness of the fiber (all HCFs for telecom networks and data transmission shall be single-mode, but ensuring this property in HC-PBGF is challenging—see Section 4.2), and group-velocity dispersion (GVD), a parameter which can be converted into the chromatic dispersion (CD) coefficient of the fiber. All those parameters are wavelength-dependent.

9. Manufacturing of Hollow-Core Fibers

9.1. Materials

Hollow-core fibers of PBGF, Kagome and ARF types are made of one material, usually chlorine-dried pure fused silica, which is strong, dimensionally stable, resistant to humidity, non-toxic, and proven in solid-core fibers. High-purity fused silica tubes for optical fiber production are commercially available [68].

Alternative materials include chalcogenide soft glasses for mid-infrared applications, and several non-crystalline polymers, in particular, PMMA [64].

Polymers, however, have the following disadvantages:

- High gas permeability, allowing for the migration of contaminants into the fiber;
- Outgassing of unreacted monomer, water, etc.;
- Absorption of water from air;
- Lack of stiffness: Young moduli of fused silica and PMMA are 72 GPa and 2.9 GPa, respectively. A 125 µm or 200 µm plastic fiber is too soft to manually handle.

9.2. Stack-and-Draw

This is the standard method for making HCFs and other microstructured fibers. The central part of fiber preform (the future photonic cladding) is assembled from glass capillaries with a 1–3 mm diameter and thin rods, drawn previously from larger, commercially available tubes, rods or plates, and consolidated via heating. This assemblage is drawn into a "cane", and jacketed with another glass tube. Complete preform is heated in electric furnace and drawn into the fiber, with polymer protective coating(s) applied [94].

Preforms for drawing NANFs and similar fibers have few parts, all of which are tubes: 7–26 for fibers with 5–8 single, nested or double-nested tubes, and one or two jacketing tubes. For comparison, the number of parts required to assemble a preform of HC-PBGF fiber like OFS AccuCore [28] or NKT HC-1550-02 [35] (Figure 6) is close to 300, resulting in substantial labor costs. The situation is similar for Kagome fibers (Figures 2 and 11).

A big problem in the fabrication of fibers including hollow cavities is the tendency of hot, softened glass to close such voids due to surface tension, with smaller voids shrinking faster and closing first. Non-circular tubes in some recently proposed ARFs with reduced confinement loss (Section 5.3, Figure 15) will likely lose their original shape.

During the consolidation of HC-PBGF preform the same phenomenon re-shapes the original assembly of round tubes into a network of (mostly) hexagonal cells constituting the photonic bandgap structure in an HC-PBGF fiber.

To prevent the deformation or collapse of tubes during the consolidation of preform and drawing of fiber, or sticking of tubes in ARF fibers, they must be selectively pressur-

ized. The typical overpressure inside holes during drawing of a ≈200 µm fused silica NANF with a relatively large tension of 4 N (increased tension reduces distortions of fiber geometry) is 15 kPa, or 15% of sea level atmospheric pressure [95], while the tolerance of this overpressure is ≤0.1 kPa [89]. A serious problem in drawing of NANFs is mid-draw contact between the tubes in the zone where the softened preform just begins to reduce its diameter, and the gas pressure dominates over the surface tension. As a result, the tubes expand too much, permanently sticking to each other and losing their circular shape when an attempt to make a fiber with closely spaced tubes (and reduced confinement loss) is made. The prevention of the deformation or sticking of tubes is described in [95].

The stack-and-draw process, while flexible, is slow due to the careful manual assembly of a preform followed by multi-stage consolidation and drawing. Low manufacturing rates, high costs, and variability in the dimensions are the result. These issues can be addressed by automation, in particular, stacking using a robot, and the application of artificial intelligence to identify irregularities via image analysis and perform corrective actions.

9.3. Extrusion of Preform

Most soft glasses can be extruded at temperatures below 400 °C. Certain pairs of soft glass and heat-resistant polymers, like PEI or fluorinated ethylene-propylene (FEP), have similar melt temperatures and can be co-extruded to make a preform, later drawn into a fiber with protective coating in a single operation. Similar materials were used in the past to make Bragg fibers—see Section 3. ARF fibers from soft tellurite glass (70%TeO_2-13%ZnO-10%BaO-7%K_2O) for power delivery at mid-infrared wavelengths, exhibiting a loss of 4.8 dB/m at 5.5 µm, were reported [96]. In this case, the preform with FEP coating was extruded at 340 °C.

The extrusion of a fused silica preform would require a temperature in the order of 1500 °C. Basalt fibers, used in tensile strength members of fiber optic cables, are successfully fabricated via the extrusion of molten basalt rock through platinum–rhodium bushings at similar temperatures: 1400–1600 °C [97]; therefore, the adoption of this method for making preforms of NANF fibers appears to be possible. Dopants decreasing fused silica viscosity, like titania (TiO_2), can reduce the required extrusion temperature.

The extrusion process for honeycomb-structured ceramic and glass products was developed and patented by Corning Glass in 1974 [98], but it is used in the production of ceramic inserts for automobile catalytic converters, not optical fibers.

9.4. Sealing of Fiber

To prevent the entry of moist air, the infiltration of liquid water when the outdoor cable is cut—up to 9 m when water pressure at typical cable laying depth of 0.6–1.2 m is considered (Section 6.4)—or the collapse of cladding during fusion splicing (Section 10.2), HCF shall be specially treated within minutes after drawing by following the steps below:

- Sealed at both ends by fusion for storage before next steps;
- Pumped with dry inert gas, like nitrogen or argon to elevated pressure;
- Tested, e.g., with OTDR, within minutes;
- Sealed at both ends by fusion for storage and shipping.

9.5. Reduction in NANF Attenuation

The lowest attenuation reported for NANF (0.22 dB/km @ 1625 nm, [49]) and DNANF (0.17 dB/km @ 1550 nm, [13]) is comparable to that if solid-core SMFs operating at the same wavelengths [30,31]. However, it is not lower. While theoretical predictions of confinement loss give values ≤0.001 dB/km [48,50], there are other loss mechanisms presented in Sections 6.2 and 6.3, primarily:

1. Leakage of light due to imperfections in cladding;
2. Surface Scattering Loss (SSL), typically 0.02–0.05 dB/km;
3. Microbending loss—specific to each fiber design;
4. Absorption by water vapor and other gas contaminants.

The lowest possible attenuation was estimated at ≈0.05 dB/km [61], unless a new design of NANF with reduced power density at the cladding inner surfaces to reduce the SSL appears.

Recommended solutions in manufacturing may include the following: (a) tighter control of geometry of capillaries to reduce confinement loss; (b) flushing newly drawn fiber with inert gas free of water vapor, methane, propane, and other absorption-inducing gases; and (c) thicker, two-layer (soft/hard) protective coating to minimize fiber microbending in cables.

10. Splicing and Termination of Hollow-Core Fibers

10.1. HCF in the SMF World

Hollow-core fibers in the near future will be connected to active and passive devices: transmitters, receivers, amplifiers, distribution frames, WDM multiplexers, etc., with optical ports designed for solid-core SMF, and two types of fiber splices will be necessary:

- HCF–HCF splices between cable sections, and for repairs;
- HCF–SMF splices at both ends of optical path, mostly to pigtails with SMFs.

Making low-loss splices of these two types is considerably different.

Single-mode HCF with MFD = 17–24 µm is not compatible with the 50/125 µm OM2/3/4/5 graded index multimode fibers [66] widely used in data centers, LANs and computer systems, primarily due to the high splice loss in the MMF-HCF direction.

Low-latency cables with single-mode HC-PBGF and NANF fibers are currently terminated with SMF pigtails at the factory [28,99] (Figure 20), while HCF–HCF joints between cable sections in long links are fusion splices. Both ends of HCF are sealed by these fusion splices and not accessible—the user only handles connectors with SMFs.

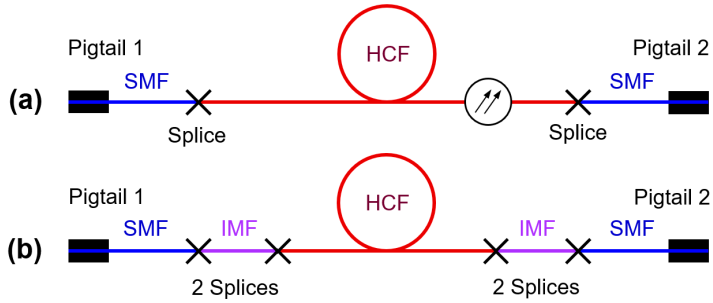


Figure 20. HCF cable with SMF pigtails: (**a**) version with single splices; (**b**) version with double splices, and short intermediate MFD fiber (IMF) inserted in the middle.

10.2. Common Issues

HCF-HCF and HCF-SMF splices shall meet the following requirements:

- Low insertion loss, preferably ≤0.25 dB;
- Low reflectivity, preferably ≤−40 dB;
- Hermeticity to prevent the contamination of HCF (Sections 6.3 and 6.4);
- Mechanical strength and long-term reliability (≥20 years).

The cladding of HCFs includes photonic structures with thin walls, down to ≈0.4 µm, and numerous holes or tubes with a diameter in the 5–75 µm range. A delicate photonic bandgap or tubular structure is prone to collapse during arc fusion, when the glass is softened and flows, and gas pressure rapidly increases. A short fusion time like 0.1–0.3 s, and carefully controlled power are mandatory [100]. There is a compromise between splice loss, rising with the length of collapse, and mechanical strength, best when the interface between fibers is fully fused [101].

Damage to photonic cladding can reduced via the following steps:

- Shortening the fusion time to ≈0.2 s so that heat does not fully penetrate the fiber's cladding;

- Reducing the arc power and current to 50–70% of value for solid-core SMF;
- Sweeping the arc along certain length of fibers to reduce inner temperature;
- Applying overpressure in all voids in the cladding.

For example, splicing NKT Photonics HC-1550-02 HC-PBGF fiber [35] (see Table 1, Figure 6) with a 125 µm jacket diameter to conventional SMF-28 fiber on an Ericsson FSU 975 fusion splicer with ≈1 mm electrode gap required pre-fusion and fusion currents of 5 mA (for 0.2 s) and 9 mA (for 0.3 s) [102], corresponding to a discharge power of ≈2.5 W and ≈4.5 W, respectively (only a part of this power is transferred to fused fibers), while currents recommended by the manufacturer for splicing two solid SMF fibers on the same machine were 10.5 mA (for 0.3 s) and 16.3 mA (for 2 s), respectively [103].

The fact that currently manufactured HC-PBGF and NANF fibers intended for data transmission and telecom networks have larger diameters, ≥200 µm (Tables 2 and 3), and require a higher arc power (approximately proportional to cross-section of glass jacket) is beneficial for fusion splicing, because a high-frequency AC electric arc at normal air pressure becomes unstable at currents below 5 mA. Otherwise, the only solution would be to use costly low-pressure arc fusion splicers or filament splicers.

Current settings adequate on a particular arc fusion splicer are generally not transferable to machines of a different type because the power generated by the arc is proportional to the voltage drop, which changes with the gap between electrodes at a rate of approx. 500 V/mm. This gap varies roughly between 1 mm and 5 mm, depending on whether the machine is designed for splicing 3 mm wide 12-fiber fiber ribbons, or only single fibers.

Advanced fusion splicing machines designed for a wide array of specialty fibers, like FITEL S184PM-SLDF ver.2 or more affordable S183PMII [104], have factory programs for splicing HCFs, rotational alignment, and even automatic adjustment of fusion parameters. Nevertheless, the user must be ready to experiment to find the best settings, dependent, in particular, on fiber diameter and jacket thickness. As most HCFs have a diameter larger than 200 µm, a large diameter cleaver is needed.

The cleaning of cut, but not sealed, HCF with a liquid solvent (isopropyl alcohol, acetone, etc.) is forbidden, as the solvent would impregnate all voids and the fiber would lose its properties. Cleaving and splicing shall be conducted in dust-free, low humidity environment, because a low pressure inside fiber [69,70] would lead to the suction of dust and wet air inside and increase the fiber loss—see Sections 6.3 and 6.4. Other solutions are different for HCF-HCF and HCF-SMF splicing.

Arc fusion splicing is applicable to fused silica fibers only. Filament splicing can also be used for joining soft glass fibers. For fibers made of polymers like PMMA, hot-melt gluing or mechanical splicing can be used.

10.3. Splicing HCF to HCF

When the spliced HCFs are identical, there is no Fresnel reflection and added loss due to MFD mismatch, described in Section 10.4. The main problem is reducing the length of the collapsed cladding and the resulting escape of light. The destruction of cladding can be prevented by using the "tack-sweep-pulse" arc fusion splicing technique, with the melting of glass only to a certain depth [105,106]. This method also works for splicing fibers of dissimilar diameters, like HCF and SMF, but requires fitting a fusion splicer with additional devices.

Butt-coupling without fusion can produce a zero-loss splice with proper fiber alignment and sealing of the joint. A possible solution is presented in Section 10.5.

To minimize splice loss, fibers shall be rotated with respect to each other prior to fusion for maximum power transfer. This is because commercial HC-PBGF fibers deliberately have non-circular cores and/or small "shunts" (Figure 5) to suppress undesirable propagation of higher-order modes [32], while NANF fibers with few tubes and gaps between them have a non-circular mode field (Figure 12b). However, the improvement during NANF splicing is limited: Suslov et al. estimated the loss of the connection of six-tube NANF to SMF with an identical MFD, but full radial symmetry, to be 0.08 dB [84].

10.4. Splicing HCF to SMF

In terms of reducing the collapse of the cladding in HCF, HCF-SMF fusion is easier than that of two HCFs, because the arc can be offset from the fiber's contact plane, directing most of the heat towards the solid fiber free of voids prone to collapse. This arrangement reduces the maximum temperature and damage in the HCF, and its efficiency has been proven with a large variety of microstructured fibers [101,107].

Zhu et al. [100] spliced SMF to NKT HC-1550-02 HC-PBGF [35] using a conventional arc fusion splicer by pumping pressurized nitrogen into HCF, completely preventing the collapse of the photonic cladding at 165 kPa internal pressure; however splice loss was still high, 1.05 dB, despite HCF and SMF-28 having a similar MFD: 9.0 μm and 10.5 μm, respectively.

The rotational alignment of fibers is not required due to the radial symmetry of SMF. However, the parameters of splice between HCF and SMF are degraded by:

- Fresnel reflection;
- MFD mismatch of fibers (see data in Tables 2 and 3).

Fresnel reflection at the interface between media with refractive indices n_1 and n_2 introduces the following return loss RL and reflection-related insertion loss IL_R:

$$RL = -20\log[(n_1 - n_2)/(n_1 + n_2)], \quad (10)$$

$$IL_R = 10\log\{1 - [(n_1 - n_2)/(n_1 + n_2)]^2\}\ [dB]. \quad (11)$$

For a butt-coupling between cleaved HCF (n_{eff} ≈1.005) and SMF (n_{eff} ≈ 1.465) with identical mode field diameters, we obtain RL = 14.60 dB and IL = 0.15 dB.

When two fibers with different mode field radii ω_1 and ω_2 are joined with perfect alignment, the joint exhibits MFD-related component of insertion loss IL_M:

$$IL_M = -20\ \log\ [(2\omega_1\omega_2)/(\omega^2{}_1 + \omega^2{}_2)]\ [dB]. \quad (12)$$

IL_M rises super-proportionally with the MFD ratio, as shown in Figure 21. When it is high, such as 2:1, which is typical when splicing SMF to NANF (Table 3), it is beneficial to insert a short length of fiber with intermediate MFD and make two splices instead of one (Figure 20b). While a single splice between fibers with 1:2 MFD ratio has the lowest loss, 1.94 dB, two splices between fibers with a 1:$\sqrt{2}$:2 MFD ratio have a combined loss of 2·0.51 = 1.02 dB.

IL_M can also be reduced via the thermal expansion of SMF core at the tip to be joined with HCF by prolonged heating to cause a diffusion of the GeO_2 dopant into areas adjacent to the core, thus increasing the core's diameter and the fiber's MFD [33].

Both components of insertion loss add up: $IL = IL_R + IL_M$.

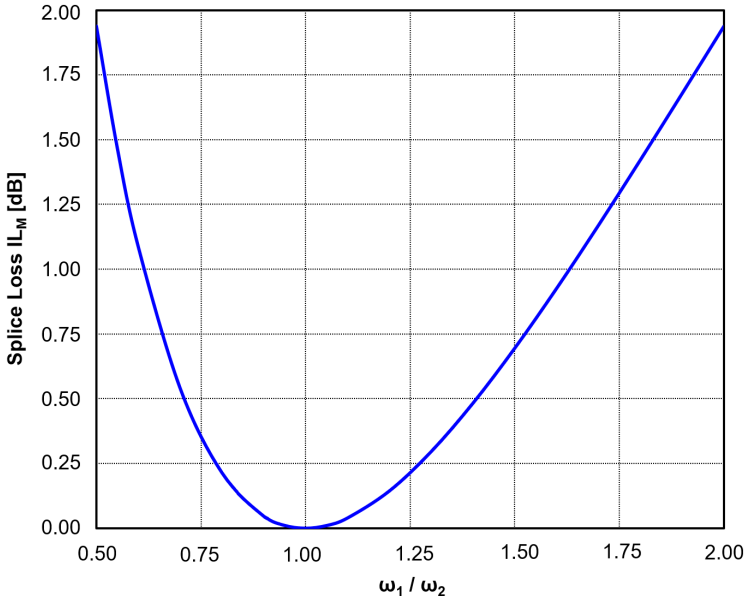


Figure 21. Splice loss component IL_M as function of MFD ratio of spliced fibers (ω_1/ω_2).

There is work on other techniques like the insertion of graded index (GRIN) lens between cleaved fibers, and fixing fibers via gluing instead of fusion. Komanec et al. [108] reported a joint loss as low as 0.30 dB between Corning SMF-28 (MFD = 10.4 µm @ 1550 nm) [30] and HC-PBGF (31.4 µm core diameter, MFD = 21.1 µm @ 1550 nm) fibers with an MFD ratio of 1:2.03. A 0.295 mm long GRIN lens made of 62.5/125 µm OM1 multimode fiber, with anti-reflection coating, served as mode size converter, with its length being critical. Its reflectivity was ≤ -30 dB. The same team later joined SMF-28 fiber to a six-tube NANF (MFD $\approx$ 24 µm) in a similar way, achieving a loss as low as 0.16 dB [84], of which half was attributed by the authors to the non-circular shape of the mode field in the NANF (Figure 18). This time, the GRIN lens was made of 50/125 µm OM2 multimode fiber. Reflectivity was reduced below -40 dB over a 60 nm bandwidth. Another MFD adaptation technique successfully tested was the inclusion of a short length of commercially available SMF-28 fiber with a core thermally expanded to MFD = 24 µm; the loss of joint was 0.21 dB.

10.5. Glass Sleeve Fusion Splicing

The destruction of HCF cladding during fusion splicing can be avoided, and splice hermeticity can be ensured in the following method invented by the authors (Figure 22).

First, a short (≈0.6–1.0 mm) capillary made of hard borosilicate glass like Pyrex 7740 [109] or other glass with a low thermal expansion coefficient is placed around one of the cleaved fibers to be spliced. Suitable capillaries are available commercially [110]. Next, the fibers are aligned (Figure 22a), later butt-coupled and (optionally) partly fused at a temperature sufficiently low to avoid damage to the cladding (Figure 22b). After this, the capillary is moved to cover the fiber contact location (Figure 22c). In the final step, the electric arc melts this capillary, heating it to approx. 1150 °C, and making it adhere to the jackets of both fibers (Figure 22d). This temperature is low enough to avoid the deformation of the fine structures in the fused silica fibers. To improve the adhesion between borosilicate and fused silica glasses, and reduce residual strains, fusion shall be followed by annealing the splice at approx. 600 °C.

Borosilicate and fused silica glasses have similar Young moduli: 64 GPa and 72 GPa; therefore, the glass cross-section of sleeve shall be similar to the jackets of the fibers. The finished splice will have a diameter small enough ($\leq$400 µm for 250 µm HCFs) to fit in standard heat-shrinkable fusion protectors designed for fibers in 900 µm buffers. Arc offset may be required when splicing SMF to HCF of different diameters to optimize the flow of borosilicate glass.

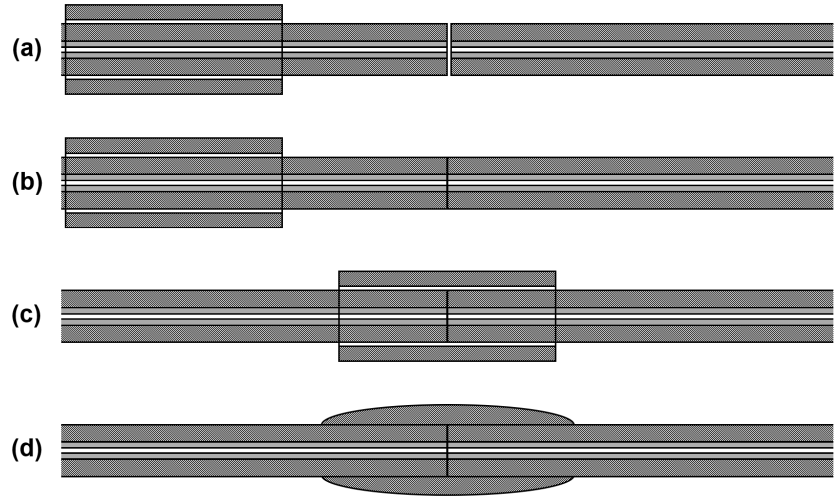


Figure 22. Fusion splicing of two HC-PBGF fibers with molten glass capillary: (**a**) fiber alignment, (**b**) push and (optional) low-temperature fusion without deformation of photonic cladding, (**c**) sliding of glass capillary over fiber contact location, (**d**) melting of glass capillary.

11. Transmission Performance of HCFs

As the commercial deployment of HCFs, with the exception of high-speed trading data links usually operating at a rate of 10 Gb/s [54], is yet to happen, we review the transmission experiments reported in literature and estimate the limits imposed by the fiber parameters.

HCFs and cables with them are available in short lengths: 1–11 km [89,111]; thus, transmission at longer distances is tested in recirculating the loop comprising length(s) of HCF and EFDA amplifier(s) compensating for the loss of fibers and passive components. In all experiments mentioned here, the operating wavelengths were within the 1550 nm window (C Band).

11.1. HC-PBGF

The record parameters reported by Kushnerov et al. [111] for a 1550 nm single-wavelength DP-QPSK link with a 19-cell HC-PBGF (single core, no shunts) were 100 Gb/s (excluding FEC) at a distance of up to 55.8 km, and 40 Gb/s up to 74.8 km, with pre-FEC BER $\leq 5 \times 10^{-2}$ in both cases. The transmission distance was limited by the interference from crosstalk between the modes. In a real network, the length of un-repeatered data link with low-loss HC-PBGF fiber (3 dB/km + 2 × 1 dB for HCF-SMF joints at both ends, see Sections 10.1 and 10.4) transceivers with a 28 dB loss budget and a 2 dB loss margin would be loss-limited to 8 km. This may suffice for fronthaul links in 5G radio networks, but not for typical telecom networks, even in a medium-sized town. Additionally, the latency added by FEC would possibly exceed the reduction in latency in the fiber (Section 12.1.2).

Mangan et al. [22] conducted a DWDM transmission test over 3.18 km long HC-PBGF fibers with six shunts (OFS AccuCore) in installed duct cable, sending 10 Gb/s channels at 33 wavelengths from 1545.32 nm to 1558.17 nm with a spacing of 50 GHz. The transceivers used NRZ line code without FEC to minimize the link's latency. BER was 10^{-15} for all channels, but attempts to add more channels at adjacent frequencies resulted in error floor due to the rise in fiber dispersion (CD or PMD) at wavelengths close to the edges of its narrow low-loss band (Figures 4 and 8). AccuCore fiber is presented in Sections 4.2 and 4.3.

The second experiment appears to reflect the best applications for HC-PBGF fibers, single-channel or low-capacity WDM links spanning short distances ($\leq$4 km) and operating at medium data rates without FEC, for latency-sensitive applications. Considering the fact that (a) the experimental link was dispersion-limited, and (b) the peculiar characteristics of chromatic dispersion of fiber used (Figure 8), one can expect much faster

single-channel transmission, e.g., 100 Gb/s, at short distances like 200 m. This is enough for most connections in a data center, LAN or campus network.

11.2. NANF

The technical data of the fibers (Table 3) suggest that NANF/DNANFs can compete with SMFs in metro/core networks, especially in large-capacity, long-distance DWDM networks where the elimination of nonlinear effects and the extension of the bandwidth are desired.

This has been confirmed by several DWDM transmission experiments summarized in Table 5. First, Nespola et al. built DWDM links with channels with a relatively low, 25 Gb/s, data rate in 2019–2021 [112–114]. In 2021, a successful transmission at 400 Gb/s and 800 Gb/s channel data rates was reported [54,115] using off-the-shelf commercial transceivers. Maximum transmission distances at 400 Gb/s satisfy the requirements for national core networks in most European countries, approx. 500–1500 km. However, new active equipment and WDM filters will be needed for networks operating at wavelengths beyond the L Band and up to ≈2100 nm—see Sections 6.2, 12.3 and 13.1.

Table 5. Summary of DWDM transmission experiments with NANF fibers in the C band.

Channel Data Rate [Gb/s]	Number of Channels	Aggregate Data Rate [Tb/s]	Line Code	Channel Spacing [GHz]	Minimum Reach [km]	Year	Ref.
25	61	1.525	PM-QPSK	50	341	2019	[112]
25	61	1.525	PM-16QAM	50	125	2019	[112]
25	61	1.525	PM-QPSK	50	618	2020	[113]
25	41	1.025	PM-QPSK	50	2760	2021	[114]
400	38	15.2	DP-16QAM [1]	100	10.25 [2]	2021	[115]
400	63	25.6	DP-16QAM [3]	75	1128	2021	[54]
800	47	38.4	No data [4]	100	126	2021	[54]

[1] Acacia 400G ZR tunable pluggable modules; [2] Test without signal recirculation; [3] Ciena WaveLogic 5 Nano 400ZR QSFP-DD coherent pluggables WL5n; [4] Ciena WaveLogic 5 Extreme 200–800G coherent optics WL5e.

Two important observations:

- The transmission distance was, in some cases, limited by Inter-Modal Interference (IMI) resulting from the coupling of optical power between the fundamental mode and higher-order modes. While a five-tube NANF with high attenuation of higher-order modes [54,114] improved the situation, the problem is not yet fully solved.
- The practical absence of Stimulated Raman Scattering (SRS) eliminated the transfer of optical power from short wavelength channels to long wavelength channels in wideband DWDM links, e.g., from C band to L band [113,115].

11.3. Fiber Ratings

Can a single figure of merit for the use of HCF in networks be defined?

In our opinion, no, primarily due to different line codes and bit rates of transponders in use and in development. For example, dispersion is critical at high bit rates (≥200 Gb/s), but not at low/medium ones, e.g., 10 Gb/s. The quality of HCF is best presented as a latency–attenuation–dispersion triangle (Figure 23a), but weights given to each parameter vary. In DWDM networks, low-loss bandwidth and nonlinearity are two additional criteria for fiber evaluation (Figure 23b).

NANF or DNANF is best in terms of transmission properties, while the advantages of HC-PBGF over SMF are limited to low latency and a superior radiation resistance. HC-PBGFs can replace graded-index multimode fibers in short links for medium bit rates (10–100 Gb/s) if low latency or radiation hardness is required. FEC and dispersion compensation can increase the bit rate and reach [111], but adds an unacceptable latency (Section 12.1.2).

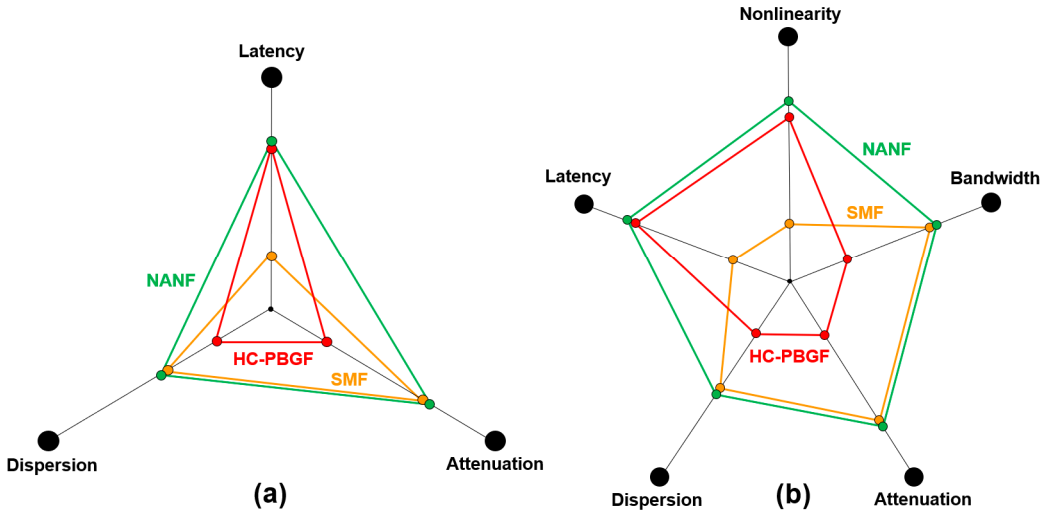


Figure 23. Simplified comparison of SMF, HC-PBGF and NANF properties important for applications in (**a**) low-latency single-wavelength links, data centers, etc., (**b**) high-capacity core or metro DWDM networks. Larger distance from center indicates better properties, e.g., lower attenuation.

12. Applications of HCFs in Networks and Systems

The current use of HCFs is mostly restricted to technical trials by operators including BT and Comcast. The exception are short data links for HST firms (Section 12.1.3).

Below, we review some applications of HCFs where their unique properties can substantially improve system performance, sorted by the following advantageous properties:

- Low latency (Section 12.1);
- Stable latency (Section 12.2);
- Wide bandwidth, low nonlinearity, and high-power capability (Section 12.3).

12.1. Low Latency Applications

12.1.1. Reduction in Latency by Using HCF

The effective refractive index (n_{eff}) of HCFs is seldom reported. The estimated values for HC-PBGF and NANF fibers are 1.005–1.010, and 1.001–1.003 at 1550 nm, respectively. Solid-core single-mode fibers [30,31] have n_{eff} in the 1.460–1.470 range, with the lowest values in Pure Silica Core Fibers (PSCF) covered by ITU-T Recommendation G.654 [78].

The latency of HCF equals 68–69% of the latency in SMF; a typical difference per unit length is 1.53 µs/km. HCF has a similar latency advantage over twisted pair and coaxial cables with solid insulation made of low-density polyethylene (LDPE).

If the network is latency-limited, the replacement of solid-core fiber with HCF can increase the reach by ≈45%, and the area covered by network from a single site by ≈100%, bringing in savings on facilities (e.g., edge data centers in a 5G network), equipment, and power.

In latency-sensitive applications, n_{eff} is not the only parameter of importance. Except for transmission over short distances (how short depends on the bit rate and line code), when the accumulated loss and dispersion (CD and PMD) are within the limits for "streamlined" transponder without time-consuming signal processing like FEC, dispersion compensation, large constellation coding/decoding, etc. (Section 12.1.2), the loss and dispersion can force network designers to adopt measures increasing the latency of data link and ultimately losing the low latency advantage of HCF, including the following:

- Adding amplifiers or repeaters to bridge excessive loss;
- Activating dispersion compensation to avoid errors;
- Activating FEC, if errors are still experienced.

When a minimum latency at all costs is the goal, for example, in HST (Section 12.1.3), the most effective solution is adding regenerators with the simplest signal path inside.

12.1.2. Latency in Transponders

The advantage of HCF as a low-latency transmission medium will be lost when high dispersion or interference from higher-order modes degrades the signal received and Forward Error Correction (FEC) is employed, introducing latency due to signal processing.

There are multiple variants of FEC. For example, the use of the Reed–Solomon (544, 514, 15) GF(2^{10}) code known as KP4 FEC (with "hard" decision) introduces latency of up to 200 ns in transponders with 25 Gb/s streams on each optical carrier and of up to 100 ns in devices with 50 Gb/s streams [116]. This corresponds to latency saved by installing 130 m and 65 m of HCF, respectively, and negates the advantage of HCF in a data center or similar facility if other transponders working over conventional fiber without FEC are available.

Latency introduced by optical transport network (OTN) equipment carrying 10 Gb/s and 100 Gb/s streams is considerably larger due to extensive signal processing. According to report of tests performed at ADVA [117], latency introduced by a 10 Gb/s transponder with RS (255,239) FEC per ITU-T G.709 standard was 6.3 µs with FEC and 2 µs without FEC for one-way transmission. Additional functions required in OTN networks add some 5 µs of latency in a 10 Gb/s transponder. The latency of a 100 Gb/s transponder 100 Gb/s utilizing newer type of FEC with "soft" decision (SD-FEC) varied within the 5.4–7.3 µs range depending on number of iterations set; the latency can be reduced at the expense of a less effective error correction. The latency introduced by these transponders is in the 2–15 µs range, equal to latency saved by the deployment of an HCF cable 1.3–10 km long.

For latency-critical applications like in data centers, dedicated 10 Gb/s transponders were developed, where FEC and other latency-generating functions like management channel are absent, or can be deactivated [118]. Certain 10 Gb/s transponders from the Infinera XTM family have their latency reduced to 4–10 ns.

12.1.3. High-Speed Trading

Electronic stock and mercantile exchanges attracted a special category of traders who built automatic "High Speed Trading" systems with lower latency 10 Gb/s connections to data centers of stock exchange operators than their competitors. The two-way latency advantage of less than 10 µs, corresponding to 1 km of SMF, is enough for a systematic winning of transactions [119–121]. Data centers serving main exchanges in the U.S., located in the Chicago and New Jersey/New York City areas, are separated by distances exceeding 1200 km, and reducing latency by 0.1% is enough.

The distances between exchanges in Chicago, NYC, London and Frankfurt, measured along geodesic lines, are about 1330 km, 5570 km and 640 km, respectively. Two-way latencies in an ordinary fiber optic network, NYC (data centers in New Jersey)—Chicago and NYC—London, are about 16 ms and 73 ms, respectively. The latencies in dedicated fiber links with straightened routes, and without aerial cables and fiber-based dispersion compensators, dropped to 13 ms and 59 ms, respectively. Several such links were built. Hibernia Express built a low-latency link from NYC to London, with a 4600 km long submarine segment and supporting 100 Gb/s services, which was activated in October 2015.

Next came microwave systems: the first Chicago—NYC radio link, activated in March 2011, had a two-way latency reduced to 8.5 ms. In April 2020, there were nine such systems. The fastest one, working in the 11 GHz band, had an estimated two-way latency of 3961.71 µs, the second one of 3962.09 µs (0.38 µs more, corresponding to a difference in route length of just 114 m, or 0.0085%) [122]. Cables with hollow-core fibers followed, although only in short feeder links to data centers of the exchanges in New Jersey and London: first with OFS AccuCore HC-PBGF in 2020 [123], and then with Lumenisity NANF in 2022.

12.1.4. Data Centers and Computers

The number of fiber optic data links in a large (hyperscale) data center can exceed a million. The total length of fibers in such a facility, assuming a 10 m average length of a patch cord (most connections are within a single rack or row of racks) and duplex

connection with 2 fibers, is 20,000 km or more. Actual link lengths vary between 2 m (intra-rack connections) and 200–400 m (cable bundles linking distant rows and sections of facility). Short- and medium-length connections, up to ca. 200 m, are carried out with 50/125 µm OM3 or OM4 multimode fibers [66]. Longer ones include single-mode fibers conforming to the ITU-T G.652.D [29] (sometimes G.652.A/ISO OS1 instead) or G.657.A [79] standards.

Besides short links and large number of connectors, another peculiarity of data centers and supercomputer facilities is their large proportion of cables terminated with multi-fiber connectors, mostly of MPO type with a capacity from 12 to 64 fibers, employed for duplex parallel data transmission. Data centers builders are large buyers of fiber optic cabling, predominantly as factory-assembled patch cords, bundles and fanouts; more than 80% of fiber optic connectors are installed in data centers, not in telecom networks.

A recent presentation of a Google engineer during OFC-2021 [124], known only from a short summary, included an estimate that latency in cabling between blocks and subsystems in a large data center reduces its throughput by 20–25%. The replacement of current fiber optic and twisted pair data cables with HFC cables and a reduction in latency by ≈31% shall increase throughput by ≈8% with the same equipment and power consumption, or reduce data center CAPEX (servers, power supply system, heating, ventilation and air conditioning equipment, floor space) and OPEX (power, cooling, maintenance) by 6–8% with respect to a facility of equal performance, but with traditional cables.

This means a large prospective market for HCFs exists, but with a low-price ceiling.

12.2. Stable Latency Applications

12.2.1. Electronic Monitoring and Stabilization of Link Latency

Since about 2005, there has been intense work carried out on the monitoring and stabilization of fiber path latency by sending a test signal to a remote site and back on a pair of closely spaced wavelengths (≈0.8 nm) via the same fiber to minimize the influence of chromatic dispersion and strain. The stability of time transfer over a 1000 km long SMF link improved to few ps was reported by several teams [125–127], and a 0.3 ps stability during 3 h was achieved during time transfer via a 96 km fiber link in a metro network [128]. This method has been adopted for long- and medium-distance time distribution, where the cost of equipment is compensated for by use of cheap, and usually already installed, SMF.

12.2.2. Radio Networks

A key example of an application sensitive to latency is fronthaul links to radio sites in a 5G cellular network. Phase synchronization of radio beams sent from multiple sites to a single user when multiple input multiple output (MIMO) technology is employed sets tight limits for differential latency in the links to all sites, as MIMO requires a matched phase for all beams aimed at the given location of the user. Without automatic monitoring and compensation of latency variations, the tolerable variation can be estimated as ±1/36th of the period of radio wave, corresponding to phase variations within ±10°. For 750 MHz, 3.6 GHz and 26 GHz frequency bands reserved for 5G networks in Poland, this corresponds to 11.11 ns, 2.31 ns and 0.32 ns, respectively.

An SMF cable has a temperature coefficient of latency of about 40 ps/km*K (Section 7.3). The difference between latencies in two aerial sections of cable attached to radio masts each 40 m long resulting from 20K difference of temperatures, e.g., when one site has sunny weather, and the other a cloudy one, is only 0.032 ns. The effect of a 10K temperature difference between two duct cables 10 km long, e.g., when one of them is laid along a pipeline, is much larger: 4 ns. The total differential latency between fronthaul links, 4.032 ns, is acceptable in a 5G network working in the 700 MHz band, but not in microwave ones.

There is ongoing work on the monitoring and compensation of variable latencies in cable links for 5G Massive MIMO networks [129], but active equipment is expensive in comparison to a short length of cable. This leaves a niche for HCFs: short links (100s m

max.), especially with exposed cables subjected to large variations in temperature. Besides 5G/6G radio sites, this includes phased-array radars and other multi-antenna systems.

12.2.3. Wide Area Multi-Antenna Systems

Because of HCF stability of latency vs. temperature (Section 7.3), it seemed likely that the space sector, specifically radio-astronomy and space radars, would become a customer installing 1000 s of km of outdoor NANF cables to build "phase stable" fiber links to antenna sites in distributed arrays. However, this prospect has probably vanished following the development of electronic latency compensation—see Section 12.2.1.

12.2.4. Time Distribution

The conclusion is identical to the one in Section 12.2.3, especially considering that all facilities in need of precise distribution/comparison of time and frequency from atomic clocks already have access to dark fibers of SMF type and Gigabit Ethernet (GbE) data links. HCFs may, however, be used in short intra-facility time distribution links.

12.3. DWDM Networks

For high-performance DWDM networks, the most important advantages of NANF/DNANF fibers over conventional SMF or PSCF fibers are:

(a) Very low optical nonlinearity, $\geq$1000$\times$ weaker than in SMF;
(b) Ability to carry high optical power;
(c) Lower attenuation and/or new low-loss bands;
(d) Low chromatic dispersion (Figure 16).

In networks spanning long distances, the low latency of NANF/DNANF fibers is beneficial too. HC-PBGFs are not suitable due to high attenuation, typically 3–5 dB/km, narrow passbands (Figure 4), and high dispersion (Figure 8)—see data in Table 2.

A gas-filled NANF has a very low nonlinear refractive index (n_2), Brillouin and Raman effects. When its attenuation is low enough ($\leq$0.20 dB/km) and the "water peak" (Figure 14) is suppressed, its use in high-capacity DWDM systems shall bring several improvements over systems with G.652.D [29] or G.654.E [78] solid-core single-mode fibers:

- Elimination of nonlinear optical effects (SPM, XPM, FWM, SRS, SBS);
- Wider bandwidth with suitable optical amplifiers;
- Increase in transmit power per channel and repeater spacing;
- Lower demand for dispersion compensation and FEC;
- Fewer amplifiers in metro and long-distance networks [130,131].

Disadvantages of NANFs in this application include:

- Impossibility of Raman amplification in the transmission fiber;
- Fire and eye safety issues due to high power carried by the fiber.

The authors of [132] analyzed the benefits of increasing the power launched into an NANF or similar fiber even to kW levels, but there is a limit imposed by the heating of splices. As presented in Section 10, it is difficult to reduce the loss of NANF-NANF fusion splice below 0.1–0.2 dB. For a 0.1 dB loss, 2.4% of the power arriving via the fiber will escape from the splice, mostly to be absorbed by the plastic parts of the splice protector and the cassette holding it; with 1 kW in the fiber, there is 24 W to dissipate, which is too much. The safe limit is around 50 W in the fiber.

Low-loss longwave bands located between 1625 nm and $\approx$2100 nm, depending on fiber design, will only be useful with suitable amplification technology. In the absence of Raman amplification in HCF, this leaves Thulium-Doped Fiber Amplifier (TDFA). The bandwidth added this way can be, by using a set of dedicated amplifiers serving several sub-bands, extended to some 1625–2050 nm (146.3–184.6 THz) [133], adding to the bandwidth of C and L bands, $\approx$1528–1610 nm (186.3–196.3 THz).

The total bandwidth usable in DWDM networks with NANFs and sets of EDFA and TDFA amplifiers can be estimated as 10 + 38 = 48 THz, approx. five times the C + L

bandwidth available today. Further capacity gains, by a factor of 4 or more, will result from the lack of signal deterioration and noise produced by nonlinear effects in the fiber, like cross-phase mixing (XPM). A higher signal-to-noise ratio enables the use of larger modulation constellations, and increasing the spectral efficiency up to ≈14 bit/s·Hz will be possible.

Restrictions imposed by noise accumulation in amplifier chains will not change, because the noise figure of optimized TDFA is similar to one of EFDA: 5–6 dB [134]. A lower attenuation of NANF like 0.05–0.10 dB/km would help, thus reducing the number of amplifiers.

The main barrier to the introduction of HCFs to metro and core DWDM networks will be cost of the fiber. However, while distances of hundreds or thousands of kilometers are typical in this segment, a single pair of new fibers shall suffice at the beginning.

13. Associated Technologies

The wide adoption of hollow-core fibers requires the availability of compatible passive and active devices, and test instruments. The disruptive novelties will likely be the following:

- Splicing of HCFS, in particular to SMFs—presented in Section 10;
- New transmission bands and optical amplifiers;
- Purging of contaminated fibers.

Additionally, an HCF-HCF connector for high-power (≈50 W) applications, compact, and sealed is desirable, e.g., for DWDM networks with optical amplifiers.

13.1. Optical Amplifiers

A suitable long-wavelength fiber amplifier, known as TDFA, was demonstrated decade ago [128], with a performance comparable to (gain, noise figure) or better (110 nm of bandwidth: 1910–2020 nm) than that of EDFA. TDFA can be modified to operate in several additional bands down to 1660 nm by co-doping active fiber with thulium and aluminum. Both amplifiers may cover almost all of the low-loss 1530–2050 nm range [134], but an increase in output power to 10s of watts (≥+40 dBm) is necessary to make full use of highly linear NANF fibers.

13.2. Test Instruments

In this area, we can expect the following novelties:

(a) Testing of loss at new wavelengths including 1800–2050 nm and 1364 nm;
(b) OTDRs able to detect low levels of Rayleigh scattering (Section 7.4);
(c) Mandatory PMD testing at the factory to detect distorted fibers.

The simplest solution to problem (b) is to increase the launched power by adding an optical amplifier like EDFA to laser in the OTDR [135], as HCF exhibits low Brillouin scattering when filled with gas at a normal atmospheric pressure or lower. Unfortunately, this brings in issues of eye safety and possible damage to active devices attached to the fiber under test.

Cables with expensive HCFs of NANF or similar type are likely to carry important traffic (HST, metro/core DWDM, links between data centers) with enhanced level of maintenance, while the ingress of humidity, e.g., through fiber break or faulty splice (Sections 6.3 and 6.4), is a particular problem. Added loss resulting from entry of water vapor is highest at wavelengths close to 1364 nm (Figure 14); therefore, the deterioration of the cable can be detected by monitoring the loss at 1364 nm. When data transmission takes place at 1550 nm, it will be possible to monitor live HCF by adding WDM multiplexers to the link.

A new instrument for the maintenance of HCF networks will be a bottle of compressed pure, dry gas like argon or nitrogen, fitted with devices for temporary attachment to a cleaved fiber and the controlled purging of it for several days or even weeks [136]. With purging, the costly replacement of a moisture-penetrated HCF cable will be avoided.

14. Conclusions

The emergence and ongoing improvements of hollow-core fibers, in particular NANFs, have opened up new prospects for a major technical change in the communications and IT sectors, primarily via a reduction in latency, the extension of optical bandwidth, the elimination of optical nonlinear effects, and an expected decrease in fiber attenuation.

The review of the features and parameters of two main types of HCFs suitable for telecom networks, data transmission and similar applications, HC-PBGF and NANF, and their comparison to conventional (solid-core) single-mode fibers has identified both advantages and shortcomings of HCFs in these applications. NANFs are definitely superior to HC-PBGFs due to a simpler design, wide bandwidth, low dispersion and low attenuation, and are already competitive with SMFs, except for cost and splicing.

We have looked at several possible applications of HCFs, analyzing the advantages of these (in their current forms) over alternative, existing technologies—or the lack of them. The most prospective are high-speed trading (currently the prime use of HCFs), DWDM networks, data centers, and radio sites with feeder cables exposed to temperature swings.

Hollow-core fibers are not yet ready for wide deployment, primarily due to low-volume and costly manufacturing. The following can be carried out to improve this situation:

- Development of more efficient and consistent manufacturing process;
- Standardization of fibers;
- Development of inexpensive and simple to use dedicated fusion splicing machines;
- Development of compatible optical amplifiers.

Author Contributions: Funding acquisition, research of the subject, collection of information (most), writing of complete draft except for Section 8, drawings, data curation—K.B. Collection of additional information, writing of Section 8, review and final editing of draft—T.O. All authors have read and agreed to the published version of the manuscript.

Funding: The work of K.B. in 2022 was funded by the Polish Ministry of Education and Science (MEiN) through support for research at National Institute of Telecommunications, Project No. 12.30.007.2 "Review of advanced designs of optical fibers, cables and networks reducing latency in optical transmission, including hollow core fibers". Work of both authors in 2023 was financed from Project No. 12.30.003.3 "Research on photonic structures for metrology, sensing and fiber optic communications".

Institutional Review Board Statement: Not applicable (study not involving humans or animals).

Informed Consent Statement: Not applicable (study not involving humans).

Data Availability Statement: This review paper was based on already existing, publicly available data. The only new data created were drawings and Section 10.5. A complete set of the digital files present in the literature used (and some extra, collected, but not used) and drawings (.ppt and png files) is stored at National Institute of Telecommunications, Warsaw. Person responsible: KB.

Acknowledgments: The support of the management of the National Institute of Telecommunications, Warsaw, for the writing of the draft in 2023 by K.B. and T.O. is acknowledged.

Conflicts of Interest: The authors declare no conflict of interest.

Abbreviations

ARF	Anti-Resonant Fiber
ARROW	Anti-Resonant Reflecting Optical Waveguide
BER	Bit Error Ratio
CAPEX	Capital Expenses
CD	Chromatic Dispersion
CL	Confinement Loss
DGD	Differential Group Delay
DNANF	Double Nested Anti-Resonant Nodeless Fiber

DWDM	Dense Wavelength Division Multiplexing
EDFA	Erbium-Doped Fiber Amplifier
FEC	Forward Error Correction
FEP	Fluorinated Ethylene-Propylene
FEM	Finite Element Method
FWM	Four Wave Mixing
GRIN	Graded Index (optical fiber or lens)
HST	High Speed Trading
HCF	Hollow-Core Fiber
HC-PBGF	Hollow-Core Photonic Bandgap Fiber
IL	Insertion Loss
ITU-T	International Telecommunication Union–Technical Standardization Sector
MCF	Multi-Core Fiber
MFD	Mode Field Diameter
MIMO	Multiple Input Multiple Output (radio network with several steerable beams)
MMFNA	Multimode Fiber (with solid core)Numerical Aperture
NANF	Nested Anti-Resonant Nodeless Fiber
OPEX	Operating Expenses
OTDR	Optical Time Domain Reflectometer
OTN	Optical Transport Network
PBGF	Photonic Bandgap Fiber
PEI	Polyetherimide
PES	Poly(ether sulfone)
PMD	Polarization Mode Dispersion
PMMA	Poly(methyl metacrylate)
POF	Polymer Optical Fiber
ppm	Part Per Million (concentration, proportion)
PSCF	Pure Silica Core Fiber
RL	Return Loss
SCW	Surface Capillary Wave
SEM	Scanning Electron Microscope
SMF	Single-Mode Fiber (with solid core and cladding)
SPM	Self-Phase Mixing
SSL	Surface Scattering Loss
TDFA	Thulium-Doped Fiber Amplifier
XPM	Cross-Phase Mixing

References

1. Kao, K.C.; Hockham, G.A. Dielectric-fibre surface waveguides for optical frequencies. *Proc. IEE* **1966**, *113*, 1151–1158. [CrossRef]
2. World's Largest Transmission Capacity with Standard Diameter Multi-Core Optical Fiber: Accelerate Multi-Core Fiber Application Using Current Standard Technology. 8 August 2017. Available online: https://group.ntt/en/newsrelease/2017/08/08/170808b.html (accessed on 21 March 2023).
3. Soma, D.; Beppu, S.; Wakayama, Y.; Sumita, S.; Takahashi, H.; Yoshikake, N.; Morita, I.; Tsuritani, T.; Suzuki, M. Trans-Pacific class transmission over a standard cladding ultralow-loss 4-core fiber. *Opt. Express* **2022**, *30*, 9482–9493. [CrossRef]
4. Debord, B.; Amrani, F.; Vincetti, L.; Gérôme, F.; Benabid, F. Hollow-Core Fiber Technology: The Rising of "Gas Photonics". *Fibers* **2019**, *7*, 16. [CrossRef]
5. Mulvad, H.C.H.; Mousavi, S.A.; Zuba, V.; Xu, L.; Sakr, H.; Bradley, T.D.; Hayes, J.R.; Jasion, G.T.; Numkam Foukua, E.; Taranta, A.; et al. Kilowatt-average-power single-mode laser light transmission over kilometre-scale hollow-core fibre. *Nat. Photonics* **2022**, *16*, 448–453. [CrossRef]
6. Yeh, P.; Yariv, A. Bragg reflection waveguides. *Opt. Commun.* **1976**, *19*, 427–430. [CrossRef]
7. Yeh, P.; Yariv, A.; Marom, E. Theory of Bragg fiber. *J. Opt. Soc. Am.* **1978**, *68*, 1196–1201. [CrossRef]
8. Birks, T.A.; Roberts, P.J.; Russell, P.S.J.; Atkin, D.M.; Shepherd, T.J. Full 2-D photonic bandgaps in silica/air structures. *Electron. Lett.* **1995**, *31*, 1941–1943. [CrossRef]
9. Yu, F.; Knight, J. Negative curvature hollow core optical fiber. *IEEE J. Sel. Top. Quantum Electron.* **2016**, *22*, 146–155. [CrossRef]
10. Komanec, M.; Dousek, D.; Suslov, D.; Zvanovec, S. Hollow-Core Optical Fibers. *Radioengineering* **2020**, *29*, 417–430. [CrossRef]
11. Richardson, D.J.; Wheeler, N.V.; Chen, Y.; Hayes, J.R.; Sandoghchi, S.R.; Jasion, G.T.; Bradley, T.D.; Numkam Fokoua, E.; Liu, Z.; Slavik, R.; et al. Hollow Core Fibres and their Applications. In Proceedings of the 2017 Optical Fiber Communications Conference and Exhibition (OFC), Los Angeles, CA, USA, 19–23 March 2017. Tu3H.1.

12. Poletti, F. Hollowcore Optical Fibres: A British Invention with Revolutionary Potential (Presentation). In Proceedings of the Telecommunications, Optics and Photonics (TOP) Conference, London, UK, 14–15 February 2022.
13. Jasion, G.T.; Sakr, H.; Hayes, J.R.; Sandoghchi, S.R.; Hooper, L.; Numkam Fokoua, E.; Saljoghei, A.; Mulvad, H.C.; Alonso, M.; Taranta, A.; et al. 0.174 dB/km Hollow Core Double Nested Antiresonant Nodeless Fiber (DNANF). In Proceedings of the 2022 Optical Fiber Communications Conference and Exhibition (OFC), San Diego, CA, USA, 6–10 March 2022. Th4C.7.
14. Fink, Y.; Ripin, D.J.; Fan, S.; Chen, C.; Joannopoulos, J.D.; Thomas, E.L. Guiding Optical Light in Air Using an All-Dielectric Structure. *J. Light. Technol.* **1999**, *17*, 2039–2041. [CrossRef]
15. Kuriki, K.; Shapira, O.; Hart, S.D.; Benoit, G.; Kuriki, Y.; Viens, J.F.; Bayindir, M.; Joannopoulos, J.D.; Fink, Y. Hollow multilayer photonic bandgap fibers for NIR applications. *Opt. Express* **2004**, *12*, 1510–1517. [CrossRef]
16. Temelkuran, B.; Hart, S.D.; Benoit, G.; Joannopoulos, J.D.; Fink, Y. Wavelength-scalable hollow optical fibres with large photonic bandgaps for CO2 laser transmission. *Nature* **2002**, *420*, 650–653. [CrossRef] [PubMed]
17. Johnson, S.G.; Ibanescu, M.; Skorobogatiy, M.; Weisberg, O.; Engeness, T.D.; Soljacic, M.; Jacobs, S.A.; Joannopoulos, J.D.; Fink, Y. Breaking the glass ceiling: Hollow OmniGuide fibers. In *Photonic Bandgap Materials and Devices*; Adibi, A., Scherer, A., Lin, S.Y., Eds.; SPIE: Bellingham, WA, USA, 2002; Proceedings of SPIE: 2002; Volume 4655. [CrossRef]
18. Benabid, F.; Roberts, P.J. Guidance mechanisms in hollow-core photonic crystal fiber. In *Photonic Crystal Materials and Devices VII, San Jose, CA, USA, 21–23 January 2008*; Adibi, A., Lin, S.-Y., Scherer, A., Eds.; SPIE: Bellingham, WA, USA, 2008; Volume 6901, p. 69010U. [CrossRef]
19. Wei, C.; Weiblen, R.J.; Menyuk, C.R.; Hu, J. Negative curvature fibers. *Adv. Opt. Photonics* **2017**, *9*, 504–561. [CrossRef]
20. Mangan, B.J.; Farr, L.; Langford, A.; Roberts, P.J.; Williams, D.P.; Couny, F.; Lawman, M.; Mason, M.; Coupland, S.; Flea, R.; et al. Low loss (1.7dB/km) hollow core photonic bandgap fiber. In Proceedings of the Optical Fiber Communication Conference 2004, Los Angeles, CA, USA, 22–27 February 2004. PD24.
21. Mukasa, K. Hollow Core Fiber Cable. *Furukawa Electr. Rev.* **2021**, *52*, 36–43. Available online: https://www.furukawa.co.jp/en/rd/review/fr052/fr52_09.pdf (accessed on 21 February 2023).
22. Mangan, B.J.; Zhu, B.; Puc, G.S.; Kremp, T.; Irid, M. Low latency transmission in a hollow core fiber cable. In Proceedings of the CLEO 2021, Virtual Event, 9–14 May 2021. STu1Q.1. [CrossRef]
23. Wegmuller, M.; Legré, M.; Gisin, N.; Hansen, T.P.; Jakobsen, C.; Broeng, J. Experimental investigation of the polarization properties of a hollow core photonic bandgap fiber for 1550 nm. *Opt. Express* **2005**, *13*, 1457–1467. [CrossRef] [PubMed]
24. Numkam Fokoua, E.; Zhu, W.; Ding, M.; Feng, Z.; Chen, Y.; Bradley, T.D.; Jasion, G.T.; Richardson, D.J.; Poletti, F.; Slavík, R. Polarization Effects on Thermally Stable Latency in Hollow-Core Photonic Bandgap Fibers. *J. Light. Technol.* **2021**, *39*, 2142–2150. [CrossRef]
25. Yu, X.; Zheng, X.; Zhang, H. PMD Measurement of Hollow-Core Photonic Bandgap Fiber by Investigating Power Penalty of Optically Generated Microwave Signals. *IEEE Photon. Technol. Lett.* **2007**, *19*, 279–281. [CrossRef]
26. Roberts, P.J.; Couny, F.; Sabert, H.; Mangan, B.J.; Williams, D.P.; Farr, L.; Mason, M.W.; Tomlinson, A.; Birks, T.A.; Knight, J.C.; et al. Ultimate low loss of hollow-core photonic crystal fibres. *Opt. Express* **2005**, *13*, 236–244. [CrossRef]
27. DiGiovanni, D.; Inniss, D.; Kremp, T.; Mangan, B.; Mikhailov, V.; Zhu, B. *AccuCore HCF Optical Cable: Low-Latency Hollow-Core Fiber Transmission Primer*; OFS Fitel White Paper; OFS Fitel LLC.: Norcross, GA, USA, 2020.
28. *AccuCore HCF Fiber Optic Cable and Assemblies*; OFS Fitel LLC.: Norcross, GA, USA, 2020.
29. ITU-T Recommendation, G. *652: Characteristics of a single-Mode Optical Fibre and Cable*; International Telecommunication Union: Geneva, Switzerland, 2016.
30. *Corning SMF-28e+ Optical Fiber Product Information PI1463*; Corning Inc.: Corning, NY, USA, 2021.
31. *Corning SMF-28 Ultra Optical Fiber Product Information PI1464*; Corning Inc.: Corning, NY, USA, 2021.
32. Mangan, B.J.; Nicholson, J.W.; Fini, J.M.; Windeler, R.S.; Meng, L.; Puc, G.; Mukasa, K. Single Mode, Polarization Maintaining Hollow Core Fibre with Significantly Improved Higher Order Mode Reduction. In Proceedings of the 2015 European Conference on Optical Communication (ECOC) 2015, Valencia, Spain, 27 September–1 October 2015; p. 0721. [CrossRef]
33. ITU-T Recommendation, G. *650.1: Definitions and Test Methods for Linear, Deterministic Attributes of Single-Mode Fibre and Cable*; International Telecommunication Union: Geneva, Switzerland, 2020.
34. Optical Connector Assemblies for Low Latency Patchcords. International Patent Application WO 2021/127032A1, 24 June 2021.
35. *Hollow-Core Fibers: Hollow-Core Photonic Bandgap Fibers (HC-800, 920, 1060, 1300, 1550)*; NKT Photonics: Boston, MA, USA, 2022.
36. Inniss, D. Low-Latency Optical Transmission: AccuCore HCF Fiber Optic Cable. In Proceedings of the Global STAC Live: High Technology in Finance, Spring 2020, Online, 2–4 June 2020.
37. Bradley, T.D.; Hayes, J.R.; Chen, Y.; Jasion, G.T.; Sandoghchi, S.R.; Slavik, R.; Numkam Fokoua, E.; Bawn, S.; Sakr, H.; Davidson, I.A.; et al. Record Low-Loss 1.3dB/km Data Transmitting Antiresonant Hollow Core Fibre. In Proceedings of the 2018 European Conference on Optical Communication (ECOC), Rome, Italy, 23–27 September 2018. [CrossRef]
38. Sakr, H.; Bradley, T.D.; Hong, Y.; Jasion, G.T.; Hayes, J.R.; Kim, H.; Davidson, I.A.; Numkam Fokoua, E.; Chen, Y.; Bottrill, K.R.H.; et al. Ultrawide Bandwidth Hollow Core Fiber for Interband Short Reach Data Transmission. In Proceedings of the 2019 Optical Fiber Communications Conference and Exhibition (OFC), San Diego, CA, USA, 3–7 March 2019. Th4A.1.
39. Jasion, T.; Bradley, G.T.; Sakr, T.; Hayes, H.; Chen, J.R.; Chen, Y.; Taranta, A.; Mulvad, H.C.; Davidson, I.A.; Wheeler, N.V.; et al. Recent breakthroughs in hollow core fiber technology. In *Next-Generation Optical Communication: Components, Sub-Systems, and Systems IX*; SPIE: Bellingham, WA, USA, 2020; Volume 11309. [CrossRef]

40. Zeisberger, M.; Hartung, A.; Schmidt, M.A. Understanding Dispersion of Revolver-Type Anti-Resonant Hollow Core Fibers. *Fibers* **2018**, *6*, 68. [CrossRef]
41. Benabid, F.; Knight, J.C.; Antonopoulos, G.; Russell, P. Stimulated Raman Scattering in Hydrogen-Filled Hollow-Core Photonic Crystal Fiber. *Science* **2002**, *298*, 399–402. [CrossRef]
42. Wang, Y.Y.; Wheeler, N.V.; Couny, F.; Roberts, P.J.; Benabid, F. Low loss broadband transmission in hypocycloid-core Kagome hollow-core photonic crystal fiber. *Opt. Lett.* **2011**, *36*, 669–671. [CrossRef]
43. Maurel, M.; Chafer, M.; Amsanpally, A.; Adnan, M.; Amrani, F.; Debord, B.; Vincetti, L.; Gérôme, F.; Benabid, F. Optimized inhibited-coupling Kagome fibers at Yb-Nd:Yag (8.5 dB/km) and Ti:Sa (30 dB/km) ranges. *Opt. Lett.* **2018**, *43*, 1598–1601. [CrossRef]
44. Wheeler, N.V.; Bradley, T.D.; Hayes, J.R.; Gouveia, M.A.; Liang, S.; Chen, Y.; Sandoghchi, S.R.; Abokhamis Mousavi, S.M.; Poletti, F.; Petrovich, M.N.; et al. Low-loss Kagome hollow-core fibers operating from the near- to the mid-IR. *Opt. Lett.* **2017**, *42*, 2571–2574. [CrossRef]
45. Amrani, F.; Osório, J.H.; Delahaye, F.; Giovanardi, F.; Vincetti, L.; Debord, B.; Gérôme, F.; Benabid, F. Low-loss single-mode hybrid-lattice hollow-core photonic-crystal fibre. *Light Sci. Appl.* **2021**, *10*, 7. [CrossRef]
46. Pryamikov, A.D.; Biriukov, A.S.; Kosolapov, A.F.; Plotnichenko, V.G.; Semjonov, S.L.; Dianov, E.M. Demonstration of a waveguide regime for a silica hollow-core microstructured optical fiber with a negative curvature of the core boundary in the spectral region > 3.5 µm. *Opt. Express* **2011**, *19*, 1441–1448. [CrossRef]
47. Kolyadin, A.N.; Kosolapov, A.F.; Pryamikov, A.D.; Biriukov, A.S.; Plotnichenko, V.G.; Dianov, E.M. Light transmission in negative curvature hollow core fiber in extremely high material loss region. *Opt. Express* **2013**, *21*, 9514–9519. [CrossRef]
48. Poletti, F. Nested antiresonant nodeless hollow core fiber. *Opt. Express* **2014**, *22*, 23807–23828. [CrossRef] [PubMed]
49. Sakr, H.; Bradley, T.D.; Jasion, G.T.; Numkam Fokoua, E.; Sandoghchi, S.R.; Davidson, I.A.; Taranta, A.; Guerra, G.; Shere, W.; Chen, Y.; et al. Hollow Core NANFs with Five Nested Tubes and Record Low Loss at 850, 1060, 1300 and 1625nm. In Proceedings of the 2021 Optical Fiber Communications Conference and Exhibition (OFC), San Francisco, CA, USA, 6–10 June 2021. F3A.4.
50. Belardi, W.; Knight, J.C. Negative curvature fibers with reduced leakage loss. In Proceedings of the OFC 2014, San Francisco, CA, USA, 9–13 March 2014; Th2A.45. ISBN 978-1-55752-993-0.
51. Sumi Rani Shaha, K.; Khaleque, A.; Hosen, S. Wideband Low Loss Hollow Core Fiber with Nested Hybrid Cladding Elements. *J. Light. Technol.* **2021**, *39*, 6585–6591. [CrossRef]
52. Wang, Y.; Chang, W. Multi-nested antiresonant hollow-core fiber with ultralow loss and single-mode guidance. *Opt. Express* **2023**, *31*, 18250–18264. [CrossRef] [PubMed]
53. Murphy, L.R.; Bird, D. Azimuthal confinement: The missing ingredient in understanding confinement loss in antiresonant, hollow-core fibers. *Optica* **2023**, *10*, 854–870. [CrossRef]
54. Saljoghei, A.; Qiu, M.; Sandoghchi, S.R.; Laperle, C.; Alonso, M.; Hubbard, M.; Lang, I.; Pasandi, M.; Chen, Y.; Petrovich, M.; et al. First Demonstration of Field-Deployable Low Latency Hollow-core Cable Capable of Supporting >1000km, 400Gb/s WDM Transmission. *arXiv* **2021**, arXiv:2106.05343. Available online: https://arxiv.org/ftp/arxiv/papers/2106/2106.05343.pdf (accessed on 11 February 2023). [CrossRef]
55. Jasion, G.T.; Bradley, T.D.; Harrington, K.; Sakr, H.; Chen, Y.; Numkam Fokoua, E.; Davidson, I.A.; Taranta, A.; Hayes, J.R.; Richardson, D.J.; et al. Hollow Core NANF with 0.28 dB/km Attenuation in the C and L Bands. In Proceedings of the 2020 Optical Fiber Communications Conference and Exhibition (OFC), San Diego, CA, USA, 8–12 March 2020. Th4B.4.
56. Zhang, X.; Song, W.; Dong, Z.; Yao, J.; Wan, S.; Hou, Y.; Wang, P. Low loss nested hollow-core anti-resonant fiber at 2 µm spectral range. *Opt. Lett.* **2022**, *47*, 589–592. [CrossRef] [PubMed]
57. Slavik, R.; Numkam Fokoua, E.; Bradley, T.D.; Tarranta, A.A.; Komanec, M.; Zvanovec, S.; Michaud-Belleau, V.; Poletti, F.; Richardson, D.J. Optical time domain backscattering of antiresonant hollow core fibers. *Opt. Express* **2022**, *30*, 31310–31321. [CrossRef] [PubMed]
58. Krzempek, K.; Abramski, K.; Nikodem, M. Kagome Hollow Core Fiber-Based Mid-Infrared Dispersion Spectroscopy of Methane at Sub-ppm Levels. *Sensors* **2019**, *19*, 3352. [CrossRef]
59. Olanterä, L.; Troska, J.; Sigaud, C.; Vasey, F.; Petrovich, M.; Poletti, F.; Wheeler, N.; Wooler, J.; Richardson, D. Gamma Irradiation of Minimal Latency Hollow-Core Photonic Bandgap Fibers. *J. Instrum.* **2013**, *8*, C12010. [CrossRef]
60. Numkam Fokoua, E.; Richardson, D.J.; Poletti, F. Impact of structural distortions on the performance of hollow-core photonic bandgap fibers. *Opt. Express* **2014**, *22*, 2735–2744. [CrossRef]
61. Numkam Fokoua, E.; Abokhamis Mousavi, S.; Jasion, G.T.; Richardson, D.J.; Poletti, F. Loss in hollow-core optical fibers: Mechanisms, scaling rules, and limits (Tutorial). *Adv. Opt. Photonics* **2023**, *15*, 1–85. [CrossRef]
62. Osório, J.H.; Amrani, F.; Delahaye, F.; Dhaybi, A.; Vasko, K.; Melli, F.; Giovanardi, F.; Vandembroucq, D.; Tessier, G.; Vincetti, L.; et al. Hollow-core fibers with reduced surface roughness and ultralow loss in the short-wavelength range. *Nat. Commun.* **2023**, *14*, 1146. [CrossRef]
63. Sakr, H.; Chen, Y.; Jasion, G.T.; Bradley, T.D.; Hayes, J.R.; Mulvad, H.-C.H.; Davidson, I.A.; Numkam Fokoua, E.; Poletti, F. Hollow core optical fibres with comparable attenuation to silica fibres between 600 and 1100 nm. *Nat. Commun.* **2020**, *11*, 6030. [CrossRef]
64. Abrate, S.; Gaudino, R.; Perrone, G. Step-Index PMMA Fibers and Their Applications. In *Current Developments in Optical Fiber Technology*; Harun, S.W., Arof, H., Eds.; IntechOpen: London, UK, 2013; pp. 177–202. [CrossRef]

65. Stawska, H.I.; Popenda, M.A.; Beres-Pawlik, E. Anti-Resonant Hollow Core Fibers with Modified Shape of the Core for the Better Optical Performance in the Visible Spectral Region—A Numerical Study. *Polymers* **2018**, *10*, 899. [CrossRef]
66. *50 µm Graded-Index OM2—Bend-Insensitive Multimode Optical Fiber (Data Sheet)*; OFS Fitel, ID: Fiber-151; OFS Fitel LLC.: Norcross, GA, USA, 2018.
67. Ciddor, P.E. Refractive Index of Air: New Equations for the Visible and Near Infrared. *Appl. Opt.* **1996**, *35*, 1566–1573. [CrossRef]
68. *Heraeus High Purity Fused Silica Tubes for Specialty Fiber Production*; Heraeus: Henau, Germany, 2020. Available online: https://www.heraeus.com/media/media/hca/doc_hca/products_and_solutions_8/optical_fiber/Fiber_Tubes_EN.pdf (accessed on 13 February 2023).
69. Rikimi, S.; Chen, Y.; Kelly, T.W.; Davidson, I.A.; Jasion, G.T.; Partridge, M.; Harrington, K.; Bradley, T.D.; Taranta, A.; Poletti, F.; et al. Internal Gas Composition and Pressure in As-drawn Hollow Core Optical Fibers. *J. Light. Technol.* **2022**, *40*, 4776–4785. [CrossRef]
70. Rikimi, S.; Chen, Y.; Bradley, T.D.; Davidson, I.A.; Sakr, H.; Taranta, A.; Harrington, K.; Poletti, F.; Petrovich, M.N.; Richardson, D.J.; et al. Comparison between the Optical Performance of Photonic Bandgap and Antiresonant Hollow Core Fibers after Long-Term Exposure to the Atmosphere. In Proceedings of the 2022 Optical Fiber Communications Conference and Exhibition (OFC), San Diego, CA, USA, 6–10 March 2022. W4E.3.
71. Bucholtz, A. Rayleigh-scattering calculations for the terrestrial atmosphere. *Appl. Opt.* **1995**, *34*, 2765–2773. [CrossRef]
72. Shardanand, A.D.; Rao, P. *NASA Technical Note TN D-8442: Absolute Rayleigh Scattering Cross Sections of Gases and Freons of Stratospheric Interest in the Visible and Ultraviolet Regions*; NASA: Washington, DC, USA, 1977.
73. NIST Basic Atomic Spectroscopic Data. Available online: https://physics.nist.gov/PhysRefData/Handbook/element_name.htm (accessed on 23 January 2023).
74. HITRAN on the Web. Available online: https://hitran.iao.ru/home and https://hitran.iao.ru/molecule/simlaunch (accessed on 23 January 2023).
75. Van Agthoven, M.A.; Fujisawa, G.; Rabbito, P.; Mullins, O.C. Near-Infrared Spectral Analysis of Gas Mixtures. *Appl. Spectrosc.* **2002**, *56*, 593–598. [CrossRef]
76. Shemshad, J.; Aminossadati, S.; Bowen, W.; Kizil, M. Effects of pressure and temperature fluctuations on near-infrared measurements of methane in underground coal mines. *Appl. Phys. B Lasers Opt.* **2011**, *106*, 979–986. [CrossRef]
77. *IEC 60793-2-50*; Optical Fibres—Part 2-50: Product Specifications—Sectional Specification for Class B Single-Mode Fibres. International Electrotechnical Commission: London, UK, 2018.
78. *ITU-T Recommendation G.654: Characteristics of a Cut-Off Shifted Single-Mode Optical Fibre and Cable*; International Telecommunication Union: Geneva, Switzerland, 2020.
79. *ITU-T Recommendation G.657: Characteristics of a Bending-Loss Insensitive Single-Mode Optical Fibre and Cable*; International Telecommunication Union: Geneva, Switzerland, 2016.
80. Hayashi, T.; Nakanishi, T.; Hirashima, K.; Shimakawa, O.; Sato, F.; Koyama, K.; Furuya, A.; Murakami, Y.; Sasaki, T. 125 µm Cladding Eight-Core Multi-Core Fiber Realizing Ultra-High-Density Cable Suitable for O-Band Short-Reach Optical Interconnects. *J. Light. Technol.* **2016**, *34*, 85–92. [CrossRef]
81. Barlow, A.J.; Payne, D.N.; Hadley, M.R.; Mansfield, R.J. Production of single-mode fibres with negligible intrinsic birefringence and polarisation mode dispersion. *Electron. Lett.* **1981**, *17*, 725–726. [CrossRef]
82. Hart, A.; Huff, R.; Walker, R.J. Optical Fiber Having Low Polarization Mode Dispersion, Due to Permanent Spin. U.S. Patent 5418881, 23 May 1995.
83. Li, M.-J.; Chen, X.; Nolan, D.A. Fiber Spinning for Reducing Polarization Mode Dispersion in Single-Mode Fibers: Theory and Applications. Optical Transmission Systems and Equipment for WDM Networking II. *Proc. SPIE* **2003**, *5247*, 97–110. [CrossRef]
84. Suslov, D.; Komanec, M.; Numkam Fokoua, E.R.; Dousek, D.; Zhong, A.; Zvánovec, S.; Bradley, T.D.; Poletti, F.; Richardson, D.J.; Slavík, R. Low loss and high performance interconnection between standard single-mode fiber and antiresonant hollow-core fiber. *Sci. Rep.* **2021**, *11*, 8799. [CrossRef]
85. Slavík, R.; Marra, G.; Numkam Fokoua, E.; Baddela, N.; Wheeler, N.V.; Petrovich, M.; Poletti, F.; Richardson, D.J. Ultralow thermal sensitivity of phase and propagation delay in hollow core optical fibres. *Sci. Rep.* **2015**, *5*, 15447. [CrossRef] [PubMed]
86. Dangui, V.; Kim, H.K.; Digonnet, M.J.F.; Kino, G.S. Phase sensitivity to temperature of the fundamental mode in air-guiding photonic-bandgap fibers. *Opt. Express* **2005**, *13*, 6669–6684. [CrossRef] [PubMed]
87. Michaud-Belleau, V.; Numkam Fokoua, E.; Bradley, T.D.; Hayes, J.R.; Chen, Y.; Poletti, F.; Richardson, D.J.; Genest, J.; Slavik, R. Backscattering in antiresonant hollow-core fibers: Over 40 dB lower than in standard optical fibers. *Optica* **2021**, *8*, 216–219. [CrossRef]
88. Numkam Fokoua, E.; Michaud-Belleau, V.; Genest, J.; Slavík, R.; Poletti, F. Theoretical analysis of backscattering in hollow-core antiresonant fibers. *APL Photonics* **2021**, *6*, 096106. [CrossRef]
89. Chen, Y.; Liu, Z.; Sandoghchi, S.R.; Jasion, G.T.; Bradley, T.D.; Numkam Fokoua, E.; Hayes, J.R.; Wheeler, N.V.; Gray, D.R.; Mangan, B.J.; et al. Multi-kilometer Long, Longitudinally Uniform Hollow Core Photonic Bandgap Fibers for Broadband Low Latency Data Transmission. *J. Light. Technol.* **2016**, *34*, 104–113. [CrossRef]
90. Marcatili, E.A.J.; Schmeltzer, R.A. Hollow Metallic and Dielectric Waveguides for Long Distance Optical Transmission and Lasers. *Bell Syst. Tech. J.* **1964**, *43*, 1783–1809. [CrossRef]

91. Duguary, M.; Kokubun, Y.; Koch, T.; Pferiffer, L. Antiresonant reflecting optical waveguides in SiO_2-Si multilayer structures. *Appl. Phys. Lett.* **1986**, *49*, 13–15. [CrossRef]
92. Litchinitser, N.M.; Abeeluck, A.K.; Headley, C.; Eggleton, B.J. Antiresonant reflecting photonic crystal optical waveguides. *Opt. Lett.* **2002**, *27*, 1592–1594. [CrossRef]
93. Vincetti, L.; Setti, V. Waveguiding mechanism in tube lattice fibers. *Opt. Express* **2010**, *18*, 23133–23146. [CrossRef]
94. Benabid, F. Hollow-core photonic bandgap fibre: New light guidance for new science and technology. *Phil. Trans. R. Soc. A* **2006**, *364*, 3439–3462. [CrossRef]
95. Jasion, G.T.; Hayes, J.R.; Wheeler, N.V.; Chen, Y.; Bradley, T.D.; Richardson, D.J.; Poletti, F. Fabrication of tubular anti-resonant hollow core fibers: Modelling, draw dynamics and process optimization. *Opt. Express* **2019**, *27*, 20567–20582. [CrossRef] [PubMed]
96. Ventura, A.; Hayashi, J.; Cimek, J.; Jasion, G.; Janicek, P.; Slimen, F.; White, N.; Fu, Q.; Xu, L.; Sakr, H.; et al. Extruded tellurite antiresonant hollow core fiber for Mid-IR operation. *Opt. Express* **2020**, *28*, 16542–16553. [CrossRef] [PubMed]
97. Ross, A. Basalt Fibers: Alternative to Glass? Composites World. 8 January 2006. Available online: https://www.compositesworld.com/articles/basalt-fibers-alternative-to-glass (accessed on 7 February 2023).
98. Bagley, R.D. Corning Glass Works: Extrusion Method for Forming Thin-Walled Honeycomb Structures. U.S. Patent US3790654A, 5 February 1974.
99. A Lumenisity White Paper: CoreSmart Hollowcore Cable Solutions. Version 1.1. Lumenisity: Romsey, UK, 2021.
100. Zhu, T.; Xiao, F.; Xu, L.; Liu, M.; Deng, M.; Seng Chiang, K. Pressure-assisted low-loss fusion splicing between photonic crystal fiber and single-mode fiber. *Opt. Express* **2012**, *20*, 24465–24471. [CrossRef] [PubMed]
101. Song, N.; Wua, C.; Luo, W.; Zhang, Z.; Li, W. High strength fusion splicing of hollow core photonic crystal fiber and single-mode fiber by large offset reheating. *Opt. Fiber Technol.* **2016**, *32*, 106–110. [CrossRef]
102. Xiao, L.; Demokan, M.S.; Jin, W.; Wang, Y.; Zhao, C.-L. Fusion Splicing Photonic Crystal Fibers and Conventional Single-Mode Fibers: Microhole Collapse Effect. *J. Light. Technol.* **2007**, *25*, 3563–3574. [CrossRef]
103. *User's Manual for the FSU 975 Single Fiber Fusion Splicer by Ericsson*; Ericsson Cables AB: Hudiksvall, Sweden, undated; Document 89ST018 R1E.
104. *FITEL S183PMII ver.2 Fusion Splicer/S184PM-SLDF ver.2 Fusion Splicer—A New Standard in the Field for High-End/Super High-End Fusion Splicing Applications*; AC2T-110021-3; Furukawa Electric: Tokyo, Japan, 2017.
105. Wooler, J.P.; Sandoghchi, S.R.; Gray, D.; Poletti, F.; Petrovich, M.N.; Wheeler, N.V.; Baddela, N.; Richardson, D.J. Overcoming the Challenges of Splicing Dissimilar Diameter Solid-Core and Hollow-Core Photonic Band Gap Fibers. In Proceedings of the Workshop on Specialty Optical Fibers and their Applications, Sigtuna, Sweden, 28–30 August 2013. W3.26. [CrossRef]
106. Wooler, J.P.; Gray, D.; Poletti, F.; Petrovich, M.N.; Wheeler, N.V.; Parmigiani, F.; Richardson, D.J. Robust Low Loss Splicing of Hollow Core Photonic Bandgap Fiber to Itself. In Proceedings of the OFC/NFOEC 2013, Anaheim, CA, USA, 17–21 March 2013. OM3I.5. [CrossRef]
107. Borzycki, K.; Schuster, K. Arc fusion splicing of photonic crystal fibres. In *Photonic Crystals—Introduction, Applications and Theory*; Massaro, A., Ed.; IntechOpen: London, UK, 2012; pp. 175–200. [CrossRef]
108. Komanec, M.; Suslov, D.; Zvánovec, S.; Chen, Y.; Bradley, T.; Sandoghchi, S.R.; Numkam Fokoua, E.R.; Jasion, G.T.; Petrovich, M.N.; Poletti, F.; et al. Low-Loss and Low-Back-Reflection Hollow-Core to Standard Fiber Interconnection. *IEEE Photonics Technol. Lett.* **2019**, *31*, 723–726. [CrossRef]
109. *PYREX and Corning Glass and Reusable Plastic Product Selection Guide*; Life Sciences, document LS-GL-001 REV14. Corning Inc.: Corning, NY, USA, March 2023; p. 115. Available online: https://www.corning.com/catalog/cls/documents/selection-guides/CLS-GL-001.pdf (accessed on 21 September 2023).
110. VitroCom Miniature Hollow Glass Capillaries (VitroTubes). CM Scientific. July 2018. Available online: https://www.cmscientific.de/wp-content/uploads/VitroCom-DataSheet.pdf (accessed on 21 September 2023).
111. Kuschnerov, M.; Sleiffer, V.A.J.M.; Chen, Y.; de Man, E.; Chen, Y.; Liu, Z.; Sandoghchi, S.R.; Jasion, G.T.; Bradley, T.; Numkam Fokoua, E.; et al. Data Transmission through up to 74.8 km of Hollow-Core Fiber with Coherent and Direct-Detect Transceivers. In Proceedings of the ECOC 2015, Valencia, Spain, 27 September–1 October 2015. Th1.2.4. [CrossRef]
112. Nespola, A.; Straullu, S.; Bradley, T.D.; Mulvad, H.C.; Hayes, J.R.; Jasion, G.T.; Gouveia, M.A.; Sandoghchi, S.R.; Bawn, S.; Forghieri, F.; et al. Record PM-16QAM and PM-QPSK transmission distance (125 and 340 km) over hollow-core-fiber. In Proceedings of the ECOC 2019, Dublin, Ireland, 22–26 September 2019. [CrossRef]
113. Nespola, A.; Straullu, S.; Bradley, T.D.; Harrington, K.; Sakr, H.; Jasion, G.T.; Fokoua, E.N.; Jung, Y.M.; Chen, Y.; Hayes, J.R.; et al. Transmission of 61 C-band Channels with L-band Interferers over Record 618km of Hollow-Core-Fiber. In Proceedings of the OFC 2020, San Diego, CA, USA, 8–12 March 2020. Th4B.5. [CrossRef]
114. Nespola, A.; Sandoghchi, S.R.; Hooper, L.; Alonso, M.; Bradley, T.D.; Sakr, H.; Jasion, G.T.; Numkam Fokoua, E.; Straullu, S.; Garrisi, F.; et al. Ultra-Long-Haul WDM Transmission in a Reduced Inter-Modal Interference NANF Hollow-Core Fiber. In Proceedings of the OFC-2021, San Francisco, CA, USA, 6–10 June 2021. F3B.5. [CrossRef]
115. Iqbal, A.; Wright, P.; Parkin, N.; Fake, M.; Alonso, M.; Sandoghchi, S.R.; Lord, A. First Demonstration of 400ZR DWDM Transmission through Field Deployable Hollow-Core-Fibre Cable. In Proceedings of the OFC-2021, San Francisco, CA, USA, 6–10 June 2021. F4C.2. [CrossRef]
116. Liu, C.Y. 100+ Gb/s Ethernet Forward Error Correction (FEC) Analysis. *Signal Integr. J.* **2019**, *9*. Available online: https://www.signalintegrityjournal.com/articles/1286-gbs-ethernet-forward-error-correction-fec-analysis (accessed on 21 September 2023).

117. Teipen, B.; Filer, M.; Grießer, H.; Eiselt, E.; Elbers, J. Forward Error Correction Trade-offs in Reduced-Latency Optical Fiber Transmission Systems. In Proceedings of the ECOC-2012, Amsterdam, The Netherlands, 16–20 September 2012. P4.07.
118. *Low Latency—How Low Can You Go? White Paper 0188-WP-RevB-0920*; Infinera: San Jose, CA, USA, 2020.
119. Lewis, M. The Wolf Hunters of Wall Street. *New York Times*. 31 March 2014. Available online: https://www.nytimes.com/2014/04/06/magazine/flash-boys-michael-lewis.html (accessed on 20 February 2023).
120. Duhigg, C. Stock Traders Find Speed Pays, in Milliseconds. *New York Times*. 23 July 2009. Available online: https://www.nytimes.com/2009/07/24/business/24trading.html (accessed on 20 February 2023).
121. Troianovski, A. Networks Built on Milliseconds. *The Wall Street Journal*. 30 May 2012. Available online: https://www.wsj.com/articles/SB10001424052702304065704577426500918047624 (accessed on 20 February 2023).
122. Bhattacherjee, D.; Aqeel, W.; Laughlin, G.; Maggs, B.M.; Singla, A. A Bird's Eye View of the World's Fastest Networks. In Proceedings of the ACM Internet Measurement Conference (IMC'20), Virtual Event, USA, 27–29 October 2020; pp. 521–527. [CrossRef]
123. Osipovich, A. High-Frequency Traders Push Closer to Light Speed with Cutting-Edge Cables. *The Wall Street Journal*. 15 December 2020. Available online: https://www.wsj.com/articles/high-frequency-traders-push-closer-to-light-speed-with-cutting-edge-cables-11608028200 (accessed on 20 February 2023).
124. Zhou, X. Low Latency for Modern Datacenter Applications. Session "Low Latency Communications—Where Do We Need It? How To Achieve It?". In Proceedings of the OFC-2021, San Francisco, CA, USA, 6 June 2021.
125. Lopez, O.; Kefelian, F.; Jiang, H.; Haboucha, A.; Bercy, A.; Stefani, F.; Chanteau, B.; Kanj, A.; Rovera, D.; Achkar, J.; et al. Frequency and time transfer for metrology and beyond using telecommunication network fibres. *Comptes Rendus Phys.* **2015**, *16*, 531–539. [CrossRef]
126. Liu, B.; Guo, X.; Kong, W.; Liu, T.; Dong, R.; Zhang, S. Stabilized Time Transfer via a 1000-km Optical Fiber Link Using High-Precision Delay Compensation System. *Photonics* **2022**, *9*, 522. [CrossRef]
127. Krehlik, P.; Sliwczynski, L.; Buczek, L.; Kolodziej, L.; Lipinski, M. ELSTAB—Fiber-Optic Time and Frequency Distribution Technology: A General Characterization and Fundamental Limits. *IEEE Trans. Ultrason. Ferroelectr. Freq. Control.* **2016**, *63*, 993–1013. [CrossRef]
128. Lu, Z.; Gui, Y.; Wang, J.; Ying, K.; Sun, Y.; Liu, L.; Cheng, N.; Cai, H. Fiber-optic time-frequency transfer in gigabit ethernet networks over urban fiber links. *Opt. Express* **2021**, *29*, 11693–11701. [CrossRef] [PubMed]
129. Bigler, T.; Treytl, A.; Loeschenbrand, D.; Zemen, T. High Accuracy Synchronization for Distributed Massive MIMO using White Rabbit. In Proceedings of the 2018 IEEE International Symposium on Precision Clock Synchronization for Measurement, Control, and Communication (ISPCS 2018), Geneva, Switzerland, 30 September–5 October 2018; pp. 118–123. [CrossRef]
130. Iqbal, M.A.; Wright, P.; Parkin, N.; Lord, A. Performance Assessment of Hollow Core Fibre in High-Capacity National Backbone Networks. In Proceedings of the Conference on Lasers and Electro-Optics (CLEO), San Diego, CA, USA, 15–20 May 2022. SM2J.1. [CrossRef]
131. Iqbal, M.A.; Wright, P.; Lord, A. Technical Study on the Viability of Hollow-Core and Ultra-Low-Loss Silica Fibres in Metro-Core Optical Networks. In Proceedings of the Optical Fiber Communications Conference and Exhibition (OFC), San Diego, CA, USA, 5–9 March 2023. Th2A.14. [CrossRef]
132. Poggiolini, P.; Poletti, F. Opportunities and Challenges for Long-Distance Transmission in Hollow-Core Fibres. *J. Light. Technol.* **2022**, *40*, 1605–1616. [CrossRef]
133. Li, Z.; Heidt, A.M.; Daniel, J.M.O.; Jung, Y.; Alam, S.U.; Richardson, D.J. Thulium-doped fiber amplifier for optical communications at 2 μm. *Opt. Express* **2013**, *21*, 9289–9297. [CrossRef] [PubMed]
134. Chen, S.; Jung, S.; Alam, S.-U.; Richardson, D.J.; Sidharthan, R.; Ho, D.; Yoo, S.; Daniel, J.M.O. Ultra-short wavelength operation of thulium-doped fiber amplifiers and lasers. *Opt. Express* **2019**, *27*, 36699–36707. [CrossRef] [PubMed]
135. Wei, X.; Shi, B.; Richardson, D.J.; Poletti, F.; Slavik, R. Distributed Characterization of Low-loss Hollow Core Fibers using EDFA-assisted Low-cost OTDR instrument. In Proceedings of the OFC-2023, San Diego, CA, USA, 24–28 March 2023. W1C.4. [CrossRef]
136. Wheeler, N.V.; Petrovich, M.N.; Baddela, N.K.; Hayes, J.R.; Numkam Fokoua, E.; Poletti, F.; Richardson, D.J. Gas absorption between 1.8 and 2.1 μm in low loss (5.2 dB/km) HC-PBGF. In Proceedings of the 2012 Conference on Lasers and Electro-Optics (CLEO), San Jose, CA, USA, 6–11 May 2012; pp. 1–2. [CrossRef]

Disclaimer/Publisher's Note: The statements, opinions and data contained in all publications are solely those of the individual author(s) and contributor(s) and not of MDPI and/or the editor(s). MDPI and/or the editor(s) disclaim responsibility for any injury to people or property resulting from any ideas, methods, instructions or products referred to in the content.